Simulations of Colloidal Quasicrystals Using a Simple Model

Jan-Willem Buurlage
Utrecht University

Supervisors:
Prof. Marjolein Dijkstra
Anjan Gantapara

Contents

Chapter 1

Introduction

The study of Quasicrystals is a very active field. Since the discovery of quasicrystals, for which Dan Shechtmann received the 2011 Nobel Prize, an increasing number of systems have been found to show quasicrystalline structures. Recently dodecagonal symmetry has been reported for a binary system consisting of metallic nanocrystals of two sizes. These nanoparticles consisted of metallic cores, coated with hydrocarbon-chains which counteract the van der Waals force and should give rise to a repulsive short-range interaction. In this research we will try to replicate this result using model as simple as possible, beginning with the square-shoulder potential and particles of a single size and increasingly making the model more complex to compare results.

This thesis is the result of 4 months of research done by Jan-Willem Buurlage as a part of the bachelor program for Math and Physics at Utrecht University. It consists of three parts.

In the first part we will describe the theoretical framework underlying this research. We will give an introduction to Quasicrystals, where we take a mathematical approach. We will discuss topics such as patterns and tilings, space groups, point groups and physical properties of quasicrystals. We will then give an introduction to Monte Carlo simulations in (soft) condensed matter. We will also explain in further detail the experimental results that led to this research.

In the second part we will explain the methods that were used to conduct this research, and show that the methods yield commonly known results for certain simple systems. We will also introduce the model we use to try and replicate the experimental results described before.

In the third part we will show the results of applying these methods to the model in question. We will discuss these results in detail, and give an outlook to possible further research.

Part I

Theoretical Framework

Chapter 2

Quasicrystals

2.1 The Discovery of Quasicrystals

Before the discovery of Quasicrystals in 1982 by Dan Shechtman, it was well established that crystals could only show certain types of symmetry. In particular, 5-fold, 10-fold and 12-fold symmetry was not possible, and mathematically this seemed to make sense as well.

The microscopic structure of crystals was theorized as early as the 17th century, when scientists such as Johannes Kepler and Robert Hooke began to work on these notions (see for example [11]). René-Just Hauy formalized these results into a modern theory of Crystallography in the early 19th century. According to this theory crystals are ordered solids, that is to say solids which are periodic at the microsopic level. Here periodicity means that you can identify a pattern (which we will call a unit cell) that repeats along some identifiable axes. Common patterns have 4-fold or 6-fold symmetry. These patterns arise everywhere. For example, a brick in a brick wall that has vertically aligned rows has 4 touching neighbors, imagine that a particle is present in the center of every brick, the crystal structure formed would have 4-fold symmetry. The more common brick wall that has every alternative row shifted then corresponds with a crystal with 6-fold symmetry. See Figure 2.1.

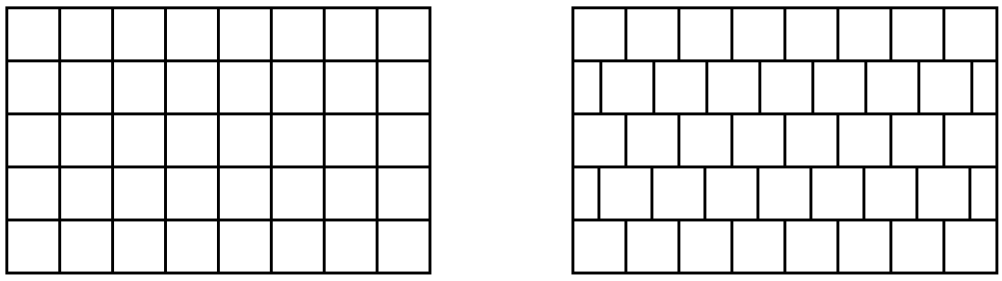

(a) Brick wall where rows are aligned.

(b) Brick wall where alternate rows are shifted.

Figure 2.1: Two brick walls, notice the difference in symmetry.

When Dan Shechtman was investigating diffraction patterns (see also: Diffraction Patterns) of a certain metallic alloy, he was surprised to find 5-fold symmetry in the Bragg-peaks of this pattern. Looking at this alloy from different angles he discovered that it showed icosahedral symmetry. It took over 2 years for the scientific community to accept and understand these results, which opened up the branch of crystallography now known as the study of quasicrystals. In 1991 the International Union of Crystallography redefined the term crystal to include quasicrystals.

2.2 Patterns and Tilings

To understand crystals and the significance of quasicrystals, we will first present some mathematical concepts that will provide us with notions and language to better grasp the differences and similarities between crystals and quasicrystals. We will begin with an introduction to patterns and tilings which are important to understand the overall structure of (quasi)crystals, as well as space- and point groups which represent the underlying symmetry of the atomic structure found in crystals. For this section we will follow the notation of the standard book on the subject *Patterns and Tilings* by *Grunbaum and Shephard* [1].

Definition 1. A **covering** $\mathcal{C}$ of the plane is a collection of subsets of $\mathbb{R}^2$ such that the union of these sets is equal to $\mathbb{R}^2$

Definition 2. A **tiling** $\mathcal{T}$ of the plane is a covering with the additional properties that individual subsets do not overlap. That is to say $U \cap V = \emptyset$ for all $U, V \in \mathcal{T}$.

Throughout this thesis we will always assume that elements of coverings are homeomorphic to a disk. For readers unfamiliar with the notion of homeomorphisms from topology it will suffice to think of regions of the plane that are free of defects like holes, gaps (that is to say, not connected) or singularities.

In particular we will be interested in **tiles** (i.e. elements of a tiling) that are polygons. We will talk about the corner points of these polygons as **vertices**. It will prove to be convenient to introduce a notation for different types of vertices, depending on the polygons which they are part of.

Notation 1. Let v be a vertex as described above. Let $\mathcal{P}$ be the set of polygons such that v is a corner-point of these polygons. We will describe this set $\mathcal{P}$ by sorting them in a clockwise fashion and writing the number of edges of these polygons between parentheses. Repeated indices are abbreviated by using superscript to denote the count (e.g. $(4^4) = (4444)$).

Example 1. A hexagonal vertex is (3^6), a square vertex is (4^4) and a vertex surrounded by hexagons can be denoted by (6^3).

Tilings can also be denoted by the vertices it is composed of. For example, the 4^4 tiling is the tiling completely consisting of squares. We will now introduce the notion of *regular tilings*, which are regular in the sense that local symmetry corresponds to symmetry of the tiling as a hole. Two tiles $T_1, T_2 \in \mathcal{T}$ are called *equivalent* if the tiling $\mathcal{T}$ admits a symmetry that maps $T_1 \mapsto T_2$. This leads to the notion of the *transitivity class* of T_1, which consists of all tiles that are equivalent to T_1. If there is only one such class in $\mathcal{T}$ then we shall call $\mathcal{T}$ *tile-transitive* (or *isohedral*).

Definition 3. A **flag** is a triplet that consists of a *vertex, edge and tile* where the vertex is part of the edge, and the edge is part of the tile. We can define the transitivity class of a flag in the same manner as we did on tiles. If $\mathcal{T}$ has a single transitivity class of flags, then the tiling is called **regular**.

It is in this sense that local symmetry and global symmetry are the same in regular tilings.

Tilings consisting of a single type of polygon are called **monohedral**. It turns out that the only monohedral regular tilings are tilings that consist of the following regular polygons: regular hexagons, squares and equilateral triangles. As mentioned Kepler researched the microscopic structure of classic crystals, and pioneered also the corresponding mathematical subject of regular tilings. We will be interested only in tilings that are *edge-to-edge*, which means that adjacent tiles have precisely one edge in common.

Before moving on to describe some common tilings by polygons we will first discuss in detail what it means for a tiling to have symmetry by the notion of space- and point groups.

2.3 Space groups, Point Groups, Lattices

Some tilings permit operations that leave the tiling unchanged, these are symmetries of the tiling or configuration. In mathematics **groups** measure symmetry in the same way numbers measure size. In this section we

will give an introduction to this mathematical description of the symmetries of tilings, and also arrive at some interesting results that give us a deeper understanding of the significance of quasicrystals and quasiperiodicty. First we will have to do some ground work and lay out some definitions. It is however not our intention to give a complete picture of group theory, and while some parts will be proven rigorously since it is relevant to the research presented in later parts, other parts will simply be discussed in a light manner.

Definition 4. A **group** is a set G along with a binary operation $\cdot$ such that

- $(g_1 \cdot g_2) \cdot g_3 = g_1 \cdot (g_2 \cdot g_3)$ $\quad (Associativity)$
- $\exists e$ such that $\forall g,\ e \cdot g = g \cdot e = g$ $\quad (Unity)$
- $\forall g,\ \exists g^{-1}$ such that $gg^{-1} = g^{-1}g = e.$ $\quad (Inverse)$

We will denote the group as the pair $(G, \cdot)$ or simply G if no confusion may arise. We will also often write $g_1 g_2 = g_1 \cdot g_2$.

An important example of a group that is directly relevant to crystals is the notion of the Euclidian group. This (infinite) group consists of all the symmetries of the plane $\mathbb{R}^2$.

Example 2. The **Euclidian group**, denoted E_2, is the group that contains all the symmetries of the plane. I.e. $G = \{f : \mathbb{R}^{\not\varepsilon} \to \mathbb{R}^2 | ||f(x) - f(y)|| = ||x - y||\}$, the set of all isometries, and the operation is given by function composition.

Familiar elements of E_2 are rotations, translations, reflections. In fact, a general element of E_2 consists of M which is either a rotation or a reflection along a line, followed by a translation along a vector v. We will denote such an element by the pair (v, M).We will also use T to denote the group containing only translations. T is a group contained in E_2, and in Group Theory one then speaks of a subgroup of E_2

Example 3. The dihedral group D_n is the symmetry group of an n-gon. It consists of n rotations, and n reflections.

A tiling can also be considered a pattern which covers the plane. An often used analogy is a wallpaper pattern covering a wall. Given such a pattern, not every symmetry of the plane will leave the pattern intact (i.e. in the same orientation or position). Restricting our group to only symmetries that leave the pattern intact we obtain a group that holds all the information on the symmetry of our tiling.

Take for example the regular tiling (6^3) and its symmetry group G. We cannot explicitly write out all the elements of the symmetry group for this pattern, since there are infinitely many since we can translate the hexagonal tiles. However, we can make the observation that all translations may be obtained by repeated translations over the vectors $\mathbf{a}, \mathbf{b}$ shown in Figure 2.2. with corresponding translations T_a, T_b. When a situation like this occurs we say that T_a, T_b **generate** the set T of translations that leave (6^3) intact. If we then add the 6 different rotational symmetries and also the reflections of (6^3) we have a full description of our group.

We will now introduce the notion of the translation subgroup and the point group.

Definition 5. Given a group G which is a subgroup of E_2, we define the **translation subgroup** to be $H = G \cap T$. Introducing the projection $\pi(v, M) = M$ which singles out the rotation/reflection component of a symmetry, we define $J = \pi(G)$ to be the **point group**.

So for the translation subgroup we only take the translations and leave the rotations and reflection out of our group. The point group only contains those symmetries that leave the origin in place. In the case of our crystal, this origin could be a single atom for example. Note that these two subgroups do not combine to make the entire group G, since symmetries where rotations and translations are combined are in neither of the two groups H, J.

An important class of subgroups of E_2 are those which are related to these patterns of tilings which much resemble wallpaper patterns. It is the first example of a general notion which for arbitrary dimension is called a space group.

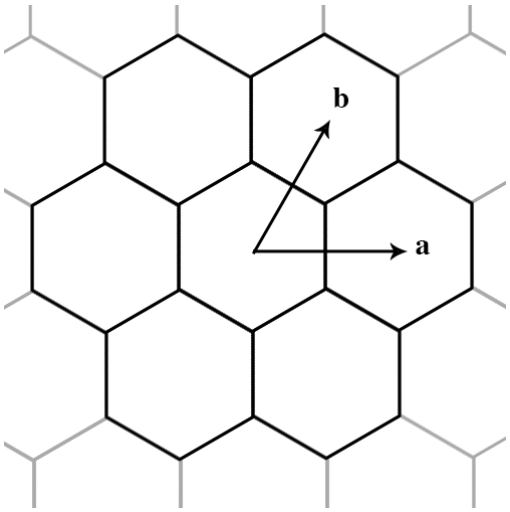

(a) The (6^3) tiling and $\mathbf{a}, \mathbf{b}$ vectors.

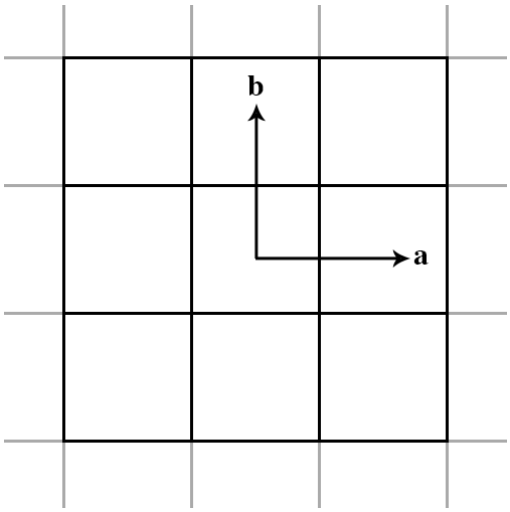

(b) The (4^4) tiling and $\mathbf{a}, \mathbf{b}$ vectors.

Figure 2.2: Two regular tilings and associated vectors which generate the translation subgroup.

Definition 6. A subgroup $G < E_2$ is called a **wallpaper group** if its **point group** is finite and its **translation subgroup** is generated by two elements.

The group representing the tiling (6^3) which we have discussed previously is an example of such a wallpaper group. It is possible to classify all the possible wallpaper groups (or more generally space groups). In two dimensions there are 17 such groups. In three dimensions there are 219 such groups. We will briefly discuss some of them in a later section, but first we will introduce the notion of a lattice and its relation to the group G.

Definition 7. The **lattice** L are the points spanned by the vectors a, b. That is to say, it consists of all points $L = \{n\mathbf{a} + m\mathbf{b} \in \mathbb{R}^2 | n, m \in \mathbb{N}\}$..

We will use this idea to prove the following theorem:

Theorem 1. A wallpaper group can only contain $2-, 3-, 4-$ or $6-$fold rotations.

Proof. We will give a geometrical proof. We know that every rotation in a wallpaper group is finite, so it is of order say q. Denote rotation over $2\pi/q$ degrees by r. For the sake of contradiction, assume $q > 6$, then $|r(\mathbf{a}) - \mathbf{a}| < |\mathbf{a}|$. So the lattice will contain points with $|a'| < |a|$ which is a contradiction. For the case $q = 5$ we see that $|r^2(\mathbf{a}) + \mathbf{a}| < |\mathbf{a}|$, which is again a contradiction with the definition of a lattice. So we conclude that it can only have $2, 3, 4$ or $6-$fold rotations. □

This result from mathematics makes rigorous what we have already seen earlier: you cannot tile the plane with pentagons. This shows that the 5-fold symmetry first observed by Shechtman in 1982 is really remarkable and raises many questions.

This idea of a lattice serves to distinguish between different patterns. Usually the different lattices are split up in 5 cases depending on the vectors $\mathbf{a}, \mathbf{b}$:

(i) Oblique: $||\mathbf{a}|| < ||\mathbf{b}|| < ||\mathbf{a} - \mathbf{b}|| < ||\mathbf{a} + \mathbf{b}||$.

(ii) Rectangular: $||\mathbf{a}|| < ||\mathbf{b}|| < ||\mathbf{a} - \mathbf{b}|| = ||\mathbf{a} + \mathbf{b}||$

(iii) Centered Rectangular: $||\mathbf{a}|| < ||\mathbf{b}|| = ||\mathbf{a} - \mathbf{b}|| < ||\mathbf{a} + \mathbf{b}||$

(iv) Square: $||\mathbf{a}|| = ||\mathbf{b}|| < ||\mathbf{a} - \mathbf{b}|| = ||\mathbf{a} + \mathbf{b}||$

(v) Hexagonal: $||\mathbf{a}|| = ||\mathbf{b}|| = ||\mathbf{a} - \mathbf{b}|| < ||\mathbf{a} + \mathbf{b}||$

For a complete classification of all wallpaper groups see for example [7]. It is also possible to classify lattices in three dimensions. This results in the 17 so called Bravais lattices which we won't discuss further here. See for example [3].

2.4 Archimedean Tilings

Recall that for a regular polygon the angle between two edges is given by $(n-2)\pi/n$ radians. Let v be a vertex, and $P_1, P_2, ..., P_r$ be some arbitrary collection of polygons. The sum of angles between edges that meet at v should be equal to 2π. This leads to the following equation:

$$\frac{(n_1 - 2)}{n_1}\pi + ... + \frac{(n_r - 2)}{n_r}\pi = 2\pi$$

It turns out that there are only 17 combinations of numbers $n_1, .., n_r$ that satisfy this equation, and thus only 17 corresponding combinations of polygons which can meet at a single vertex. This (disordered) collection of polygons around a vertex v is called the species of the vertex. In 4 of these cases there are two distinct ways to order these polygons (not including cyclic permutation). Two relevant examples for us are the (3^2434) and (3^34^2) vertices and corresponding tiles. (see also: Frank-Kasper phases). This results in 21 ordered collections of polygons, referred to as vertex types. There are 21 distinct types of vertices.

Definition 8. Only 11 tilings exist such that all vertices are of the same type. Collectively these are called the **Archimedean tilings**.

These tilings where first introduced by Kepler in 1619.

2.5 Relation to Crystals

We will now begin relating these results to the theory of crystals. In a crystal (or any spatial distribution or **configuration** of particles for that matter) we have atoms inside a volume. In a perfect crystal the configuration of these atoms is completely regular, Although in practice this will never happen, in crystallography this is happily ignored, and we only consider these perfect arrangements [3]. Atoms do not necessarily sit exactly on lattice points, but there is a certain local structure called a **basis** (insert Figure) within which atoms can by described by their position R_j relative to the lattice point. Because we are usually looking at three dimensional volumes, this means there exist vectors $\mathbf{a}, \mathbf{b}, \mathbf{c}$, and these vectors span a volume called the **primitive cell**. They can be any one of the Bravais lattices mentioned above. We can then describe the position of each and every atom by three integers $m, n, k \in \mathbb{Z}$ and the position R_j of the atom within the primitive cell. This position is given by $m\mathbf{a} + n\mathbf{b} + k\mathbf{c} + R_j$.

For convenience, we can split these three dimensional lattices up in two-dimensional planes. For every type of lattice there are an infinite amount of *families of planes* associated with them. For the most simple lattice, which we will call cubic, where $\mathbf{a} \perp \mathbf{b} \perp \mathbf{c}$ and they are all of equal length (i.e. the vectors coincide with the standard basis of $\mathbb{R}^3$) for example, we can see that we can take planes at infinitely many different angles. These planes are then characterized by the density of lattice points, and the interplanar spacing. Every family of planes can be identified with a triplet of indices called the **Miller Indices**. These can be found for a given plane as follows:

1. Choose a coordinate system
2. For a given plane, calculate the intersection with the axes x, y, z.

3. For vectors $a\mathbf{e_1}, b\mathbf{e_2}, c\mathbf{e_3}$ that span the unit cell and coincide with the chosen basis, calculate the numbers $a/x, b/y, c/z$ and express this triplet as the set of smallest possible integers h, k, l.

We will then denote these planes by the triplet (hkl), with the convention that e.g. negative h will be denoted by $\overline{h}$. The reason to look at 2-dimensional planes in 3-dimensional configuration is because they are far easier to study.

2.6 Diffraction Patterns

To verify that a configuration is indeed crystalline, we need an experimental verification method. The most common way is by looking at the diffraction pattern of a configuration. In fact, a crystal is defined to be a configuration which diffraction pattern has discrete Bragg-peaks. A diffraction pattern is the result of interference effects caused by the elastic scattering of electrons, X-rays or neutrons by the atoms in the configuration.

Let the sample be irradiated with a parallel beam of monochromatic rays with wavevector $\mathbf{k}$. The particles in the sample will scatter these beams by acting as a secondary source of waves. We will consider the family of parallel beams with wavevector $\mathbf{k}'$. Where $|\mathbf{k}| = |\mathbf{k}'|$. From the geometry of the system (in particular the difference in path length of the two beams) it follows that the phase difference between rays in this family caused by a particle at position $\mathbf{r}_i$ and an arbitrary position in the sample $\mathbf{R}$ is given by:

$$\Delta\phi = (\mathbf{k}' - \mathbf{k}) \cdot (\mathbf{r} - \mathbf{R})$$

The amplitude of this beam originating from $\mathbf{r}_i$ is proportional to $\exp(i\Delta\phi)$. Denote $\mathbf{q} = \mathbf{k}' - \mathbf{k}$. Summing over all pairs of particles i, j we find that the intensity (which is the square of the modulus of the amplitude) for a family of beams at an angle θ is proportional to the structure factor which is given by:

$$S(\mathbf{q}) = \left\langle \frac{1}{N} \sum_{i,j}^{N} (\mathbf{k}' - \mathbf{k}) \cdot (\mathbf{r_i} - \mathbf{r_j}) \right\rangle$$

Given vectors $\mathbf{a}, \mathbf{b}, \mathbf{c}$ spanning our unit cell, we can look at a parallelepiped sample spanned by the vectors $\{M\mathbf{a}, N\mathbf{b}, P\mathbf{c}\}$. Then for each plane $(n_1 n_2 n_3)$ there will be an associated diffracted beam which will give a maximum (Bragg-peak) in the diffraction pattern. This is the reason periodic crystals necessarily have a discrete diffraction pattern. It also shows why it was so surprising that Shechtman found a discrete diffraction pattern that did not correspond with any known periodic crystal. [3]

When a system is completely unordered, the structure factor $S(\mathbf{q})$ will be equal to unity, and in a perfect crystal it will be different to zero if $\mathbf{q}$ lies along a lattice plane. For a non-perfect crystal, the amount $S(\mathbf{q})$ varies from unity will then be a measure of the order of the system [3]. We can introduce the radial distribution function $g(r)$ which is a measure for the chance to find a particle at a distance r from another particle. It turns out that this function is the Fourier transform of the structure factor $S(q)$. Because Bragg-peaks correspond to the lattice planes (hkl) introduced before, one can see that when atoms are not perfectly aligned to this plane the Bragg-peak will die out. The less dense such a plane is, the faster the Bragg-peak will die out.

2.7 Quasiperiodicity

To introduce the concept of quasiperiodicity we will look at the Fibonacci sequence. In fact, this sequence generalizes to a 2-dimensional sequence which has a close relation to the famous Penrose Tilings which in turn is often used as a model for quasicrystals.

Let us first describe a system with long range order in 1-dimension. The density function for a system where particles are placed on a one dimensional lattice with lattice constant a is given by:

$$\rho_1(x) = \sum_n \delta(x - na)$$

Where δ is the Dirac-delta. If we add more particles at a lattice with lattice constant αa where α is an irrational number, then the system will be aperiodic and the density function will then be given by

$$\rho_2(x) = \sum_n \delta(x - na) + \sum_m \delta(x - m\alpha a)$$

The Fourier components of ρ_1, ρ_2 are given by F_h and $F_{hh'}$ respectively, where

$$F_h = \sum_h \delta(Q_h - 2\pi h/a) \qquad F_{hh'} = \sum_{h,h'} \delta(Q_{hh'} - 2\pi/a(h + h'/a)$$

And where h, h' are two independent integers. The **Fibonacci chain** is a one dimensional aperiodic sequence of numbers. It is an example of a 1-dimensional aperiodic sequence that has a discrete diffraction pattern. It is defined as follows:

Definition 9. The **Fibonnaci chain** F_n is defined as $F_n = F_{n-2} + F_{n-1}$ with $F_0 = F_1 = 1$.

It can be shown that $F_n/F_{n-1} \to \tau$ for $n \to \infty$. Here, τ is the *golden ratio*, which is a famous irrational number with many interesting properties. When analyzing the Fourier transform of this chain, one will notice sharp diffraction peaks which will fill the space in a dense manner. That is to say, the Fibonacci has (infinitely many) sharp diffraction peaks. Because it is aperiodic, yet has a discrete diffraction pattern one says that the sequence is quasiperiodic.

2.8 Frank-Kasper phases

There are some common patterns found in dodecagonal quasicrystals that are convenient to denote with with a single letter. Often the corresponding Frank-Kasper phases are used. We will use 4 of such patterns throughout this thesis. Two of these are presented below in Figure 2.3. with the corresponding notation that was introduced above. The other two are $H = (3^3 4^2)$ that is relevant because it is often encountered as a wetting layer between hexagonal (Z) crystals and other regions, and the square tiling (4^4).

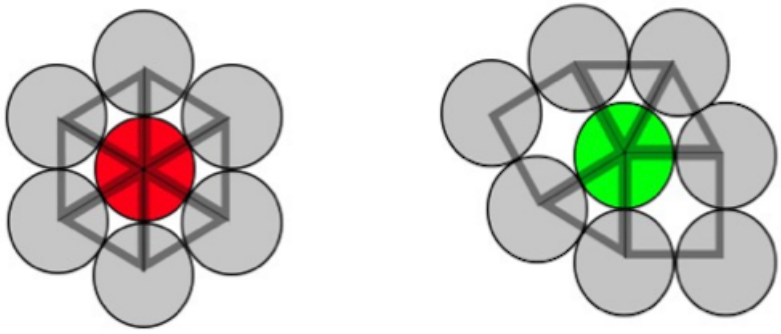

(a) A Z particle and the corresponding (3^6) tile.

(b) A σ particle and the corresponding (3^2434) tile.

Figure 2.3: Two examples of particles named after the corresponding Frank-Kasper phases.

2.9 Ideal Dodecagonal Quasicrystal

There are different ways to produce a quasicrystal in theory. Since we are interested in dodecagonal quasicrystals (DDQC), we will primarily discuss methods. A popular method is by using random tilings of squares and triangles. In fact, the Archimedean tilings $(3^2434), (3^34^2)$ result in a configuration that resembles a quasicrystal in some ways. Often these tilings are used as a starting point, and a technique involving a 'zipper' is used to turn this tiling to a quasicrystalline approximant. See also [4].

What is often done is to use a dodecagonal pattern as a building block, and stack these blocks in a varieties of ways. Stacking these patterns randomly, you can obtain a quasicrystalline configuration. See Fig. 2.4a.

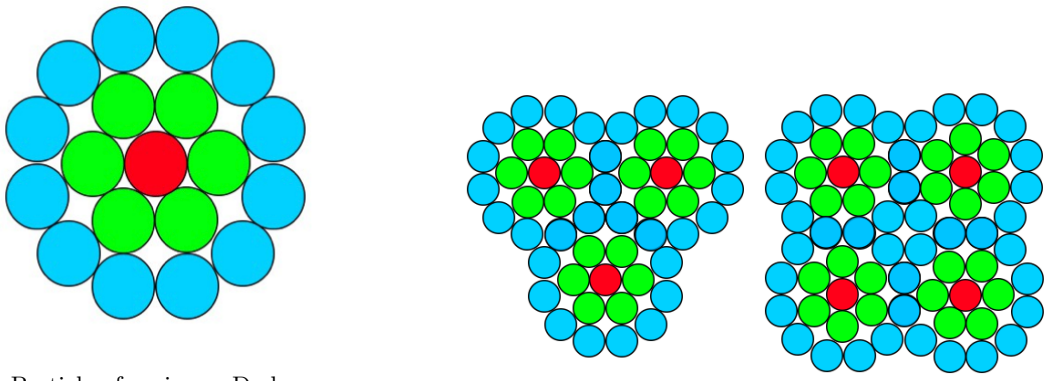

(a) Particles forming a Dodecagonal pattern.

(b) Two of the many ways to stack a dodecagonal pattern.

Figure 2.4: Periodic boundary conditions; constructing a torus from a square.

A common method for generating a DDQC is by using the (extended) Schlochtmann inflation rules. It produces deterministic 12-fold symmetric square-triangular tilings. Beginning with a random square/triangle tiling one can replace each vertex with the dodecagonal pattern of Figure 2.4a. (possibly rotated over $\pi/12$ radians, depending on the local geometry). This results in a system with a clear 12-fold diffraction pattern (See also: [2] Supplementary A). This is an example of an often used technique where simple motifs are locally replaced by a more complex ones.

2.10 Examples of Quasicrystals

In this section we will describe a couple of systems that are known to form quasicrystals, either in experiments or in simulation.

2.10.1 Hard Tetrahedra

Resent results have shown quasicrystalline configurations in simulations of a system of hard tetrahedra [5]. This example is particularly remarkable because it is a relatively simple three-dimensional system with only a hard-core potential.

These results have shown that a strictly repulsive and simple potential can lead to quasicrystalline structures in simulations. We will try to build up on this and also require that our potential is isotropic and two-dimensional. Also, hard tetrahedra of small sizes are hard to make in the lab, which makes it hard to replicate these results in experiments.

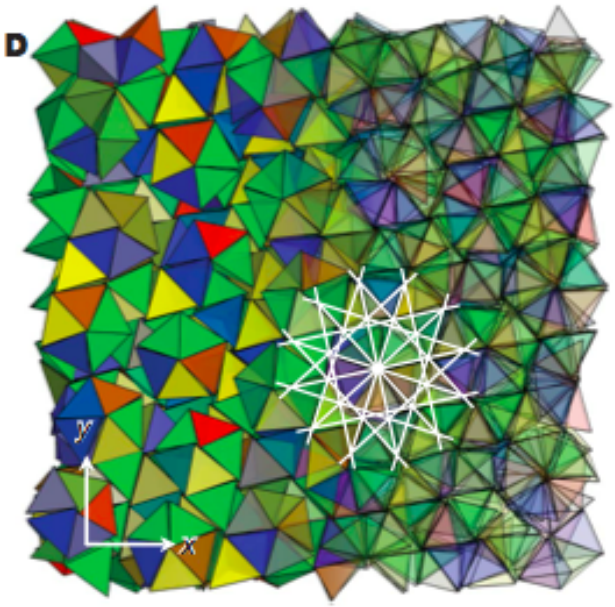

Figure 2.5: Image showing the dodecagonal pattern in a configuration consisting of hard tetrahedra. Taken from [5].

2.10.2 Coated metallic nanocrystals

The result that motivates a large part of this research are from an experiment where quasicrystalline regions were observed in a binary system metallic nanocrystals that were coated with oleic acid. Quasicrystalline regions were found for binary mixtures of a number of different materials. Therefore it is thought that the material does not really matter. The size ratio of the two different particles for which quasicrystalline phases were observed was always around $\gamma = 0.43$ regardless of the materials used [6].

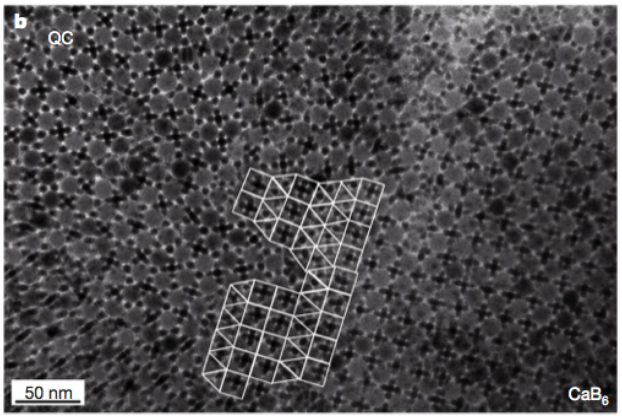

Figure 2.6: The interface between a region of a square crystal, and the quasicrystalline region mentioned above. Notice also the $(3^3 4^2)$ wetting layer which has been marked with white polygons. Taken from [6].

As we will discuss later on, we will try to replicate the results of this experiment in simulations, using isotropic pair-potentials. The most important assumption we make is that it is not necessary for the system to be binary.

2.10.3 Patchy particles

Another example of a system where quasicrystalline configuration have been found in simulations is one of patchy particles with 5 and 7 patches [2].

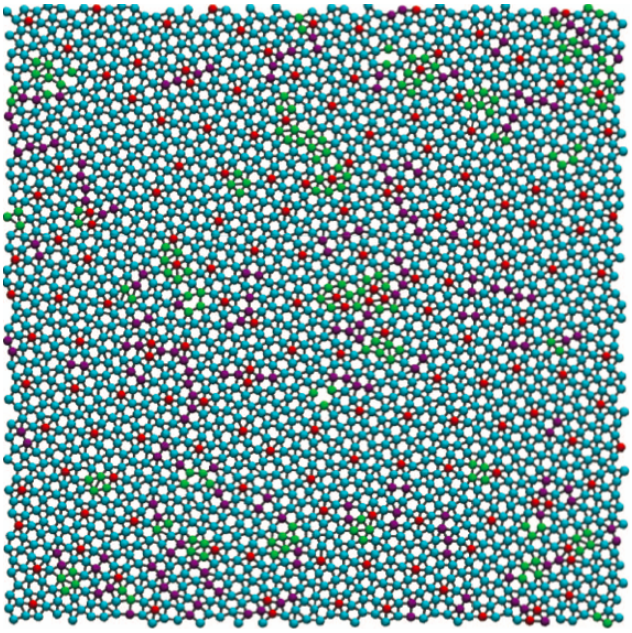

Figure 2.7: Image showing the dodecagonal pattern in a configuration consisting of patchy particles. The apparently random stacking of the dodecagonal patterns of Figure 2.4a is obvious. Taken from [2].

This anisotropic potential has significantly different behaviour depending on the patch width. A small enough patch width is required for σ particles to form. For the right patch width this model has the added benefit that σ particles have lower energy than H particles, which is necessary to form a DDQC.

Chapter 3

Monte Carlo Methods

In this section we will describe the method used for the simulation. In particular it will serve as an introduction to Monte Carlo methods. We will begin with a description of a Monte Carlo simulation in the canonical (NVT) ensemble. We will make use of a lot of (hopefully) familiar results from Thermodynamics and Statistical Physics, see for example [8]. For more information on Monte Carlo methods see the book by Frenkel [9] or the lecture notes for the course Computational Soft Condensed Matter at Utrecht University [10].

Our system will be described by a Hamiltonian of the form:

$$H(\mathbf{r}^N, \mathbf{p}^N) = \sum_{i=1}^{N} \frac{\mathbf{p}_i^2}{2m} + U(\mathbf{r}^N) \tag{3.1}$$

Recall that for observables A that are independent of the momentum (i.e. they depend only on the position of the particles, so $A(\mathbf{r}^N)$), the canonical ensemble average is given by

$$\langle A \rangle = \frac{\int d\mathbf{r}^N A(\mathbf{r}^N) \exp\left(-\beta U(\mathbf{r}^N)\right)}{\int d\mathbf{r}^N \exp\left(-\beta U(\mathbf{r}^N)\right)} \tag{3.2}$$

Trying to solve these integrals numerically however can be difficult and extremely time-consuming. Even when the number of particles is low these integrals will be nearly impossible to evaluate. This is why we need an alternative way to calculate the ensemble average $\langle A \rangle$.

3.1 Metropolis Scheme

The reason why evaluating the integrals in (3.2) is so slow is because most of the configurations we consider will have a very low Boltzmann weight (that is to say, $\exp(-\beta U(r_i^N))$ will be close to zero). If we can find a way to only evaluate the integral at likely configurations then we will have much less space to cover. First, let us consider a random sequence of n configurations $\{r_i \mid 0 \leq i \leq n\}$. In this discrete case the ensemble average will be given by

$$\langle A \rangle = \lim_{n \to \infty} \frac{\sum_{i=1}^{n} A(r_i^N) \exp(-\beta U(r_i^N))}{\sum_{i=1}^{n} \exp(-\beta U(r_i^N))} \tag{3.3}$$

However, if we are able to generate these configurations depending on their Boltzmann factor (to be precise: r_i is in the sequence with a probability proportional to $\exp(-\beta U(\mathbf{r}_i^N))$ then the ensemble average can be written as:

$$\langle A \rangle = \frac{\sum_{i=1}^{n} A(r_i^N)}{n} \tag{3.4}$$

This way of evaluating, by generating configurations according to their Boltzmann factor, is called Metropolis sampling. Because it is impossible to generate infinite sequences in simulations the average is approximated by making n very large.

3.2 Acceptance Rules

A method to generate $\mathbf{r}_i^N$ according to their Boltzmann weight is as follows: we start with an initial configuration that has a Boltzmann weight that is non-vanishing (i.e. a likely configuration). From this starting point which we will denote with o, we define the next configuration in an iterative way. We generate a new configuration n, for example we can change the position of a random particle. The next configuration in our sequence will then either be n or o depending on whether we accept the move. We will denote the probability distribution $f_c(r_i^N) = \exp(-\beta U(r_i^N))$. We require a certain acceptance rule which has to satisfy all the following conditions:

1. *Ergodicity:* All possible configurations can in principle be visited.
2. *Boltzmann weight:* The number of points in any configuration o should be proportional to $f_c(o)$.
3. *Balance:* In equilibrium the *average number of accepted trial moves leaving* o should be equal to the *average number of trial moves back to* o.

Let us denote the chance to accept a move (by displacing a single particle) from state o to the new state n by $\beta(o \to n)$. Many choices for β satisfy the three conditions above, but a common one is of Metropolis:

$$\beta(o \to n) = \begin{cases} \exp\left(-\beta(U(n) - U(o))\right) & f_c(n) < f_c(o) \\ 1 & \text{otherwise} \end{cases}$$

What this means in practice is that one will generate a random real number in the interval $[0, 1]$, and accept the move if it is lower than $\beta(o \to n)$ and reject it otherwise. Before we move on we should first talk about generating random numbers.

3.3 Generating Random Numbers

In this section we will discuss the generation of random numbers. It is far from trivial to generate random numbers with a computer, because of the logical and deterministic nature of the machine. Many standard libraries shipped with programming languages contain a random number generator (for example `rand()` found in `<random.h>` for the *C* language), but these stock random number generators are often too simple for our application because of the large number of cycles our program runs for. For example, the aforementioned `rand()` function has a period of 2^{32} in some implementations, which is far smaller than the amount of steps a sufficiently complicated Monte Carlo simulation requires. We will therefore use the Mersenne Twister random number generator (RNG) because of its long period and reasonable speed. This RNG is often used for Monte Carlo simulations.

3.4 Periodic Boundary Conditions

Because the system size of real physical systems are often very large, trying to mimic this in simulation would be very slow. Instead, what is often done is looking at only a small portion of the system and making the

assumption that the rest of the system will behave similarly. An elegant way to do this is by using periodic boundary conditions.

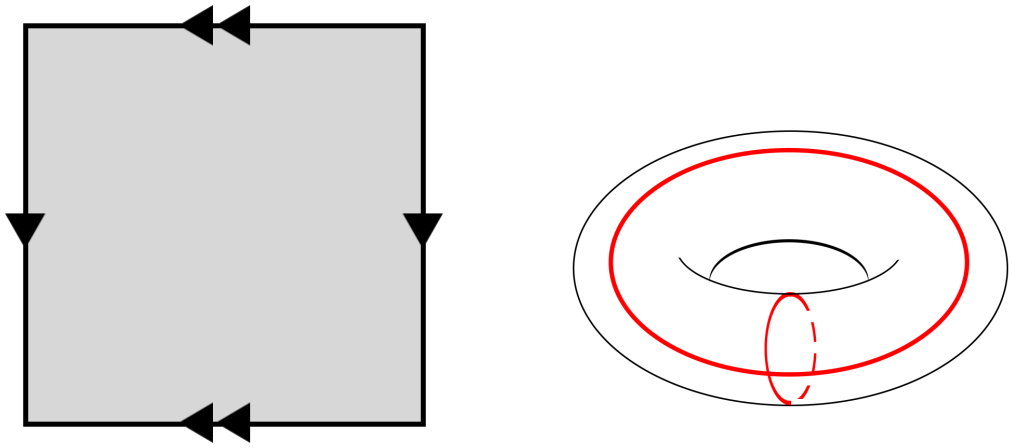

(a) Glueing the sides of a square.

(b) A torus with its short and long circles.

Figure 3.1: Periodic boundary conditions; constructing a torus from a square.

We will write L for the length of one side of the box. Every particle is repeated in all dimensions at distances $L, 2L, 3L, etc.$ When calculating differences we agree to always take the nearest image of a particle, and use that to calculate the distance. What this means mathematically (in two dimensions) is that we confine our particles to the surface of a torus. Figure 3.1a. shows why this is the case; the sides of the square can be thought of as being identifiable with a point at the same position on the other side. The sides can be thought of as being glued together (think about folding a sheet of paper). This is a very common way to construct a torus in topology. When you move a particle vertically you can think of it as going around the short circle of a regular torus, and when you move a particle horizontally you can think of it as moving along the long circle of a torus.

3.5 Isobaric-Isothermal Scheme

It is often convenient to not keep the volume V fixed, but instead the pressure P. This is the NpT-ensemble, and has been used for simulating a large variety of systems. We will consider our volume to be in contact with a large reservoir with which it can exchange heat freely. If this reservoir is sufficiently large then it can be shown that our acceptance rule for a change of volume (*volume move*) where the sides go from length $L \to L'$ becomes:

$$\beta(o \to n) = \exp[\beta(U_n - U_o) + P(V' - V) - N\beta^{-1} \ln(V'/V))]$$

Where $V = L^3$, $V = L'^3$. If the move gets accepted, then the coordinates of the particle will scale in accordance with the length change $L \to L'$. This scheme was used extensively throughout this research. We will measure the 'time' in our system as discrete steps called 'Monte Carlo cycles' (MCS) which consist of N particle moves, and one volume move as described in this section.

Part II

Methods and Models

Chapter 4

Simulations

4.1 Monte Carlo Method

The Monte Carlo Method used is the Isobaric-Isothermal scheme which is described in detail in the first part of this thesis. A computer program was written which takes the following input parameters: $MCS, \epsilon, \lambda, p_0, p_1, \Delta p$ and after equilibrating outputs the current configuration every 1000 Monte Carlo cycles as well as the pressure, box size and other relevant information on the system. It will run for the pressures $p = p_0$ up to $p = p_1$ with Δp increments.

4.1.1 Technical Details

Many other (helper)programs were written to ease the process of dealing with the large amount of generated configurations and systemdata. Separate programs were written for identifying particles (see also the corresponding section), counting particles, and for easily making plots for all the gathered data.

The main simulation program was run for many different parameters at once on a computer-cluster. The energy of the system was plotted and checked to see if the system was equilibrated. Configurations were then both checked by hand and automatically by coloring the different particles and calculating the diffraction pattern.

A complete collection of source- and scriptfiles that were used for this research can be found on the following webpage: `https://github.com/jwbuurlage/colloidal-quasicrystals`.

4.1.2 Example: Hard Spheres

We have applied this method to a three-dimensional system of hard spheres with diameter σ. We have used the Monte Carlo method in the NpT-ensemble as described above to measure the density at a given pressure. Inverting this relation and plotting it against the Carnahan-Starling equation:

$$\beta p \sigma^3 = \frac{1 + \eta + \eta^2 - \eta^3}{(1 - \eta)^3} \tag{4.1}$$

and using the relation $pv_0 = \eta$ where $v_0 = \frac{\pi\sigma^3}{6}$ is the volume of a single hard sphere particle, and $\beta = 1/k_B T$ with k_B Boltzmann's constant and T the temperature, yielded the following results:

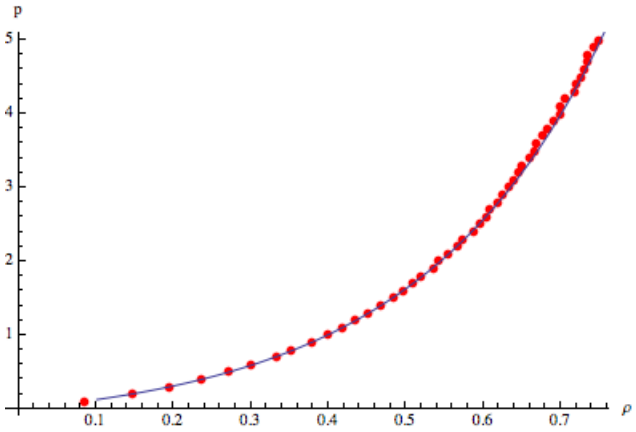

Figure 4.1: The equation of state, $\beta p\sigma^3$ versus ρ/σ^3, obtained from simulation of hard spheres with diameter σ. Each red dot is a data point form our simulations, and these are compared with the Carnahan-Starling equation of state, see Eq. 4.1.

4.1.3 Example: Hard Disks

To verify that this method also works in two-dimensions, we have applied the Monte Carlo method in the NpT-ensemble to hard disks. We have compared the $p - \eta$ relation with analytical results which yielded the following results:

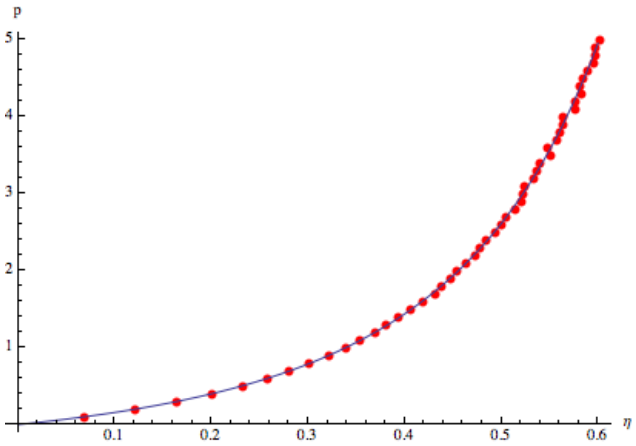

Figure 4.2: A plot comparing values found in our simulations of hard disks with those found in literature. Each red dot is a datapoint from our simulations, and these are compared analytical results

4.2 Identifying Particles

When running simulations and analyzing the configurations that result from these simulations it is often convenient to visually distinguish particles that have different **local neighborhoods**. For example, in an hexagonal crystal a particle may be touched by 6 particles, whereas in a square crystal it is only touched by 4. There is no best way to classify particles by their local neighborhoods, it all depends on the length scales that are present in your system. For example, in a system that is close to hexagonal it is probably best to only consider particles that are touching or very close to touching the particle in question. We will present three different ways of classifying particles here.

The first one, which we will call **nearest neighbors** is a method where for each particle p_i you count the particles p_j that are within a certain cutoff radius r^*. This is an easy way to distinguish between many neighborhoods that make up regular tilings.

The second one will make use of two length scales and will be called **nearest and next-nearest neighbors**, and it is the one used for most of the configurations we will generate. Here we count for each particle the particles p_j that are within a certain cutoff radius r_1^* and the particles p_k that are within the range $r_1^* < .. < r_2^*$. We can denote a pair $(5, 2)$ this way which will serve as our classification system.

Another method of classifying, which we have come across in many papers on quasicrystals, we will call the **common neighbor principle**. Here we only have a single cutoff radius again, and we count for each particle p_j how many neighbors we have in common with this particle. This results in a certain signature, e.g. (222222) for the (6^3) tiling, which we can use as our classification system. The benefit of this system is that it distinguishes between σ and H particles, both of which are very common in quasicrystalline configurations.

4.3 Tools

While writing the hard-sphere and hard-disk code we have written an accompanying program which utilizes OpenGL to view the configuration as it progressed in realtime. Later configurations were viewed using a stock configuration viewer developed by the SCM research group at Utrecht University, and was also used to produce all the images of configurations found in the next part RESULTS. The diffraction patterns were obtained using code written at Utrecht University.

Chapter 5

Square-shoulder model

As we briefly touched upon in the introduction, the goal of this research is to replicate the results of experimental findings of dodecagonal symmetry in a system of metallic nanocrystals with hydrocarbon chains **??**. We will initially try to model this system using hard-disks of a single size, equipped with a square shoulder potential. This potential is given by:

$$\beta U_{sq}(r) = \begin{cases} \infty & r < \sigma \\ \epsilon & \sigma \leq r < \lambda\sigma \\ 0 & r \geq \lambda\sigma \end{cases}$$

We have applied the NpT-ensemble Monte Carlo method to this model. Forcing $k_bT = 1$ and letting $N = 1800$ under periodic boundary conditions, our model is completely characterized by 3 parameters, namely λ, ϵ and the pressure p. We have extensively explored the parameter space and we will present the results in the next part.

As we have seen, dodecagonal quasicrystals have two natural lengthscales because of the presence of triangles and squares of particles in the system. Because the crystal structure of hard disks is hexagonal, and because a hexagon consists of 6 triangles we want to use our model to generate squares in the system. We have done this by setting the λ smaller than the 2nd natural length scale which is $\sqrt{2}\sigma$. For most of the results $\lambda = 1.4$ is used and unless stated differently this is the λ used in the results.

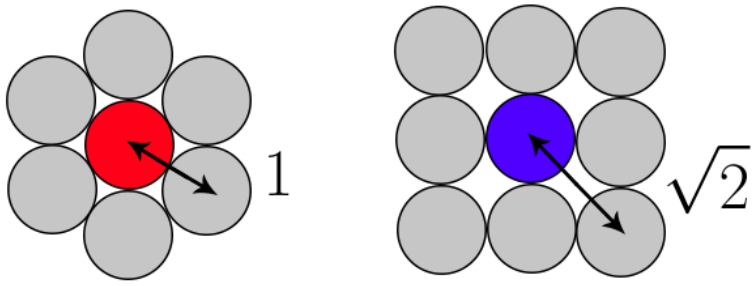

Figure 5.1: Two possible neighborhoods in our model. The Z particle has an energy of 6ϵ, whereas the square particle has an energy of 4ϵ, given $\lambda = 1.4$.

Different structures are biased for different values in parameter space. In a hardsphere system a hexagonal crystal forms for high pressures. The square-shoulder potential introduces a repulsive interaction which

makes it so that square patterns have lower energy than hexagonal patterns. This means that we can expect patterns such as the σ and H particles we discussed before, to form.

Part III

Results

Chapter 6

Results

Monte Carlo simulations have been run for a large variety of points in the parameter space for various system sizes. Because of the presumed aperiodicity of the structures formed one prefers to simulate a system as large as possible. Because of computational complexity and the limited time in which this research had to be done we compare simulations where $N = 1800$ with smaller systems where $N = 1250$ for the same region of parameter space. Configurations are analyzed by different means. Plots were generated which show the particle type ratio for a single system of $N = 1250$ particles under gradually increasing pressure (see also the section on Identifying Particles). Configurations were taken from simulations with a larger system size $N = 1800$. From the dodecagonal pattern shown in Fig. 2.4a. we can see that for a DDQC we expect there to be a large amount of σ particles (colored green) compared to Z particles (colored red). We expect there to be a very small amount of square particles S (colored dark blue). We also would like to minimize the amount of unidentified particles U (colored light blue), for they are indicative of fluid regions. We will present the results here for the plane $\lambda = 1.4$ ordered by increasing energy.

So for a quasicrystalline region we would expect the σ particles to form the predominant neighborhood, followed by hexagonal particles which form the center of the dodecagonal pattern. We will analyze the orientational symmetry of the system by looking at the diffraction pattern. To make sure the system is in equilibrium we checked the energy of a system as a function of the time, measured in Monte Carlo cycles (MCS). We will analyze the behavior of large regions of the system by means of particle-ratio plots where we look for a region where σ-particles form the predominant neighborhood. It is important to note that our classification does not distinguish σ and H particles, however from the configurations it can be seen that the vast majority of particles are indeed σ particles. However, H particles were seen to form a wetting layer between hexagonal and square crystalline regions.

For reference the different local neighborhoods of interest are shown in Fig. 6.1.

6.1 Results for $\epsilon = 1$

Simulations have been run for $\beta p\sigma^3 \in [1, 110]$, which resulted in configurations that were not unlikele those found in a regular hard-disk system. It was however clear that crystallization started to take place at higher pressures than normal, as a result of the repulsive potential.

As we can see from Figure 6.2. no significant amount of σ or H particles form in this range, and for higher regions there is a high fraction of Z particles. There was no immediate reason to explore configurations for this energy further, since from the figures presented here we see that a quasicrystal is unlikely to form for $\epsilon = 1$. However, we do expect that σ and square particles are increasingly more common for higher energies (see also Fig. 5.1.)

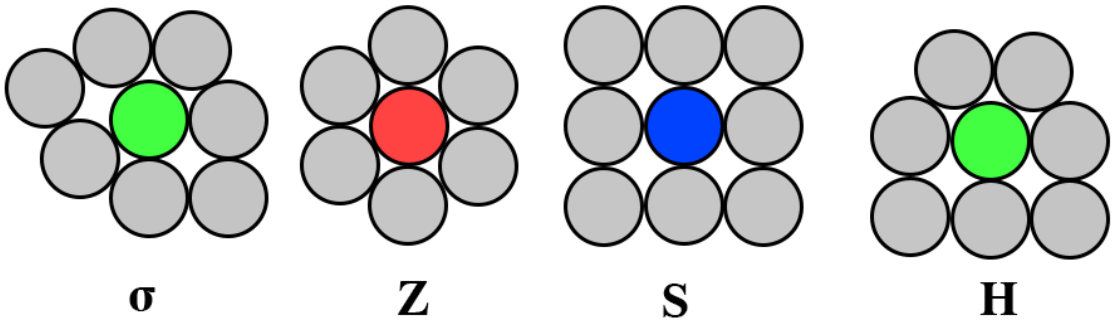

Figure 6.1: The different local neighborhoods (also referred to as particle types) mentioned in the text.

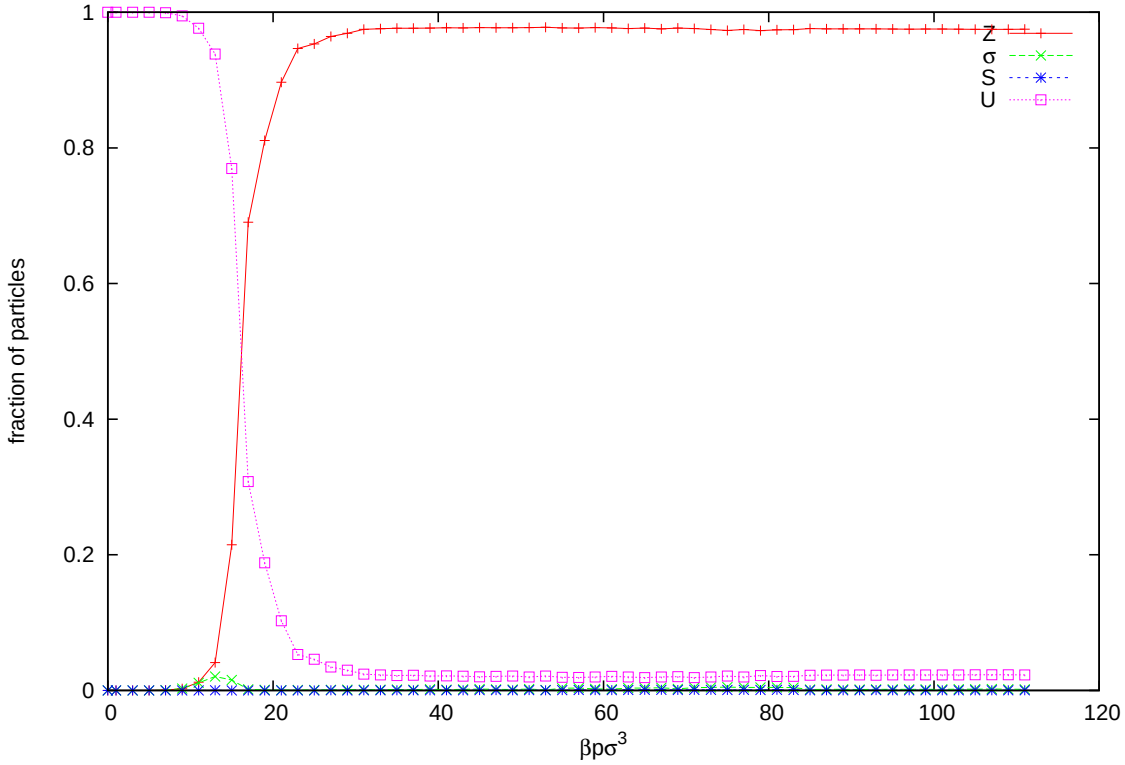

Figure 6.2: The fraction of particles of different types as a function of $\beta p\sigma^3$ for $\epsilon = 1$ for a system of $N = 1250$ particles with gradually increasing pressure.

6.2 Results for $\epsilon = 3$

At higher energies, beginning around $\epsilon = 3$, we immediately see that there is a formation of σ and H particles, which already starts for relatively low pressures ($\beta p\sigma^3 = 30$). There is an interesting region

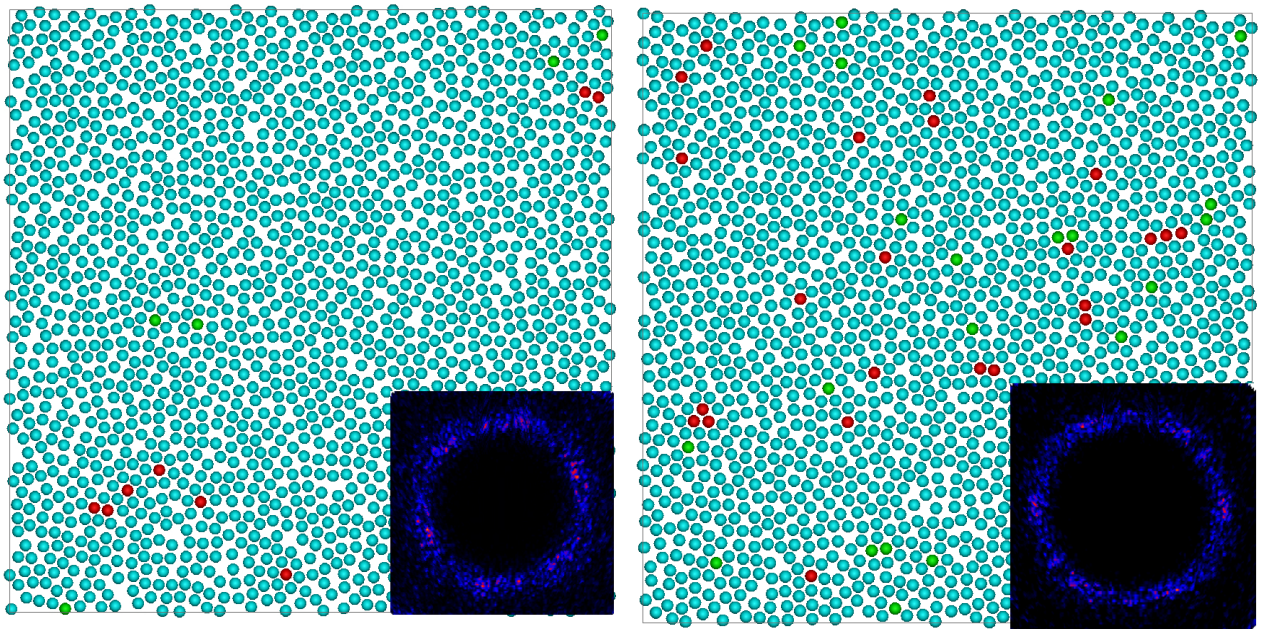

(a) $\beta p\sigma^3 = 12$

(b) $\beta p\sigma^3 = 12$

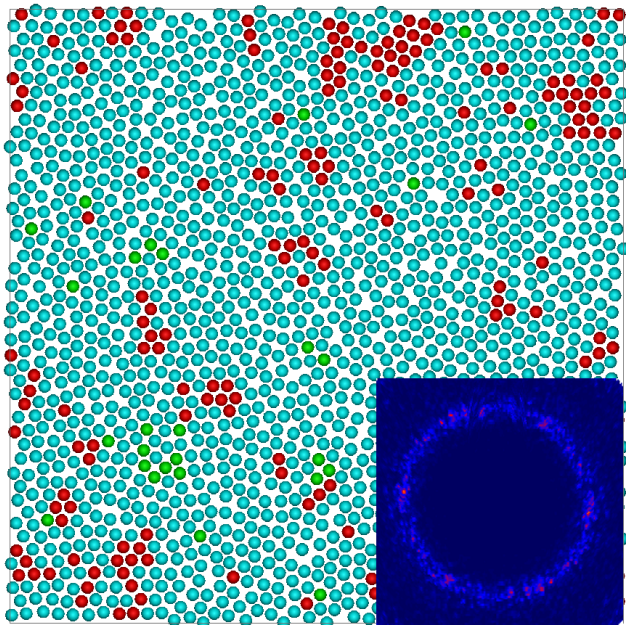

(c) $\beta p\sigma^3 = 14$

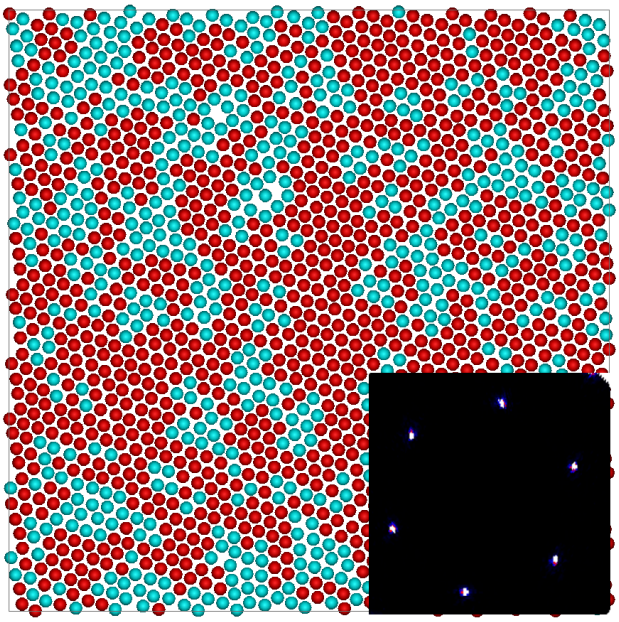

(d) $\beta p\sigma^3 = 16$

Figure 6.3: A selection of configurations for $\epsilon = 1$ at different pressures with the corresponding diffraction patterns for a system of $N = 1800$ particles.

starting at $\beta p\sigma^3 = 30$ where the amount of unidentified particles is very low compared to the amount of σ particles. There is also a good amount of Z particles formed, and this amount increases with pressure. The density of the system in this region however is too low, which means the system is not crystallizing. This is also shown by the diffraction patterns of the configurations. For higher pressures the system starts to form a hexagonal crystal and it seems very unlikely that a DDQC would form for pressures higher than $\beta p\sigma^3 = 90$, since the system clearly favors Z particles there. Interestingly, in a single run with $N = 1250$ the system seemed to form a very stable configuration where the majority of the system consisted of σ particles. It is

likely that the system got 'stuck' since the system dynamics are relatively slow for this particular system. From these results we can predict that for higher energies the system will be in this σ-favored region until higher pressures, and possibly the system will get dense enough for it to crystallize.

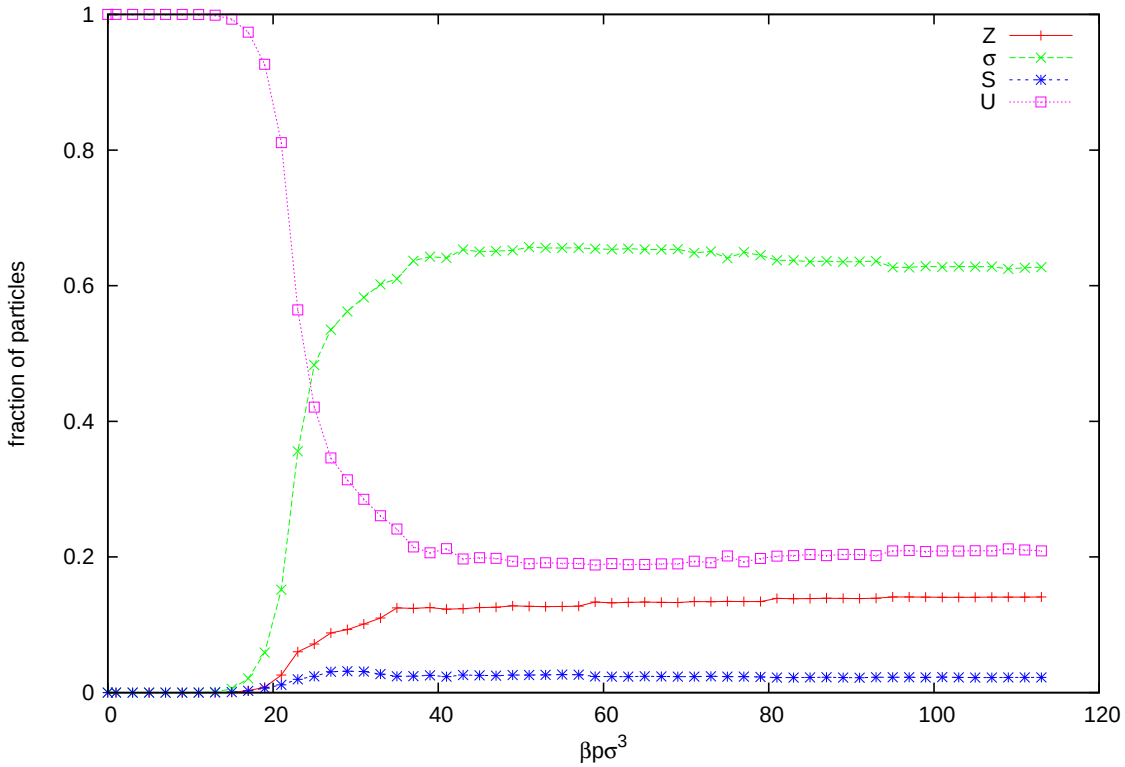

Figure 6.4: The fraction of particles of different types as a function of $\beta p\sigma^3$ for $\epsilon = 3$ for a system of $N = 1250$ particles with gradually increasing pressure. The structure formed around $\beta p\sigma^3 = 35$ seems to stable until much higher pressures in this particular run.

6.3 Results for $\epsilon = 4$

For $\epsilon = 4$ we can see more clearly than for lower energies that the system will exhibit square patterns for relatively low pressures $p \approx 30$. In fact, starting at this energy, there is a region where a square crystal would possibly be stable. We also see a large amount of σ and H particles start to form before the system starts to crystallize to a hexagonal crystal. At high pressures we see distinctive polycrystalline phases. Interestingly some of these configurations where shown to have 12-fold diffraction patterns.

6.4 Results for $\epsilon = 5$

We see that for lower pressures $\beta p\sigma^3 \approx 30$ there is a distinctive region where large chunks of square crystaline regions start to form. For higher pressures there is a large region, relative to lower energies, where σ particles

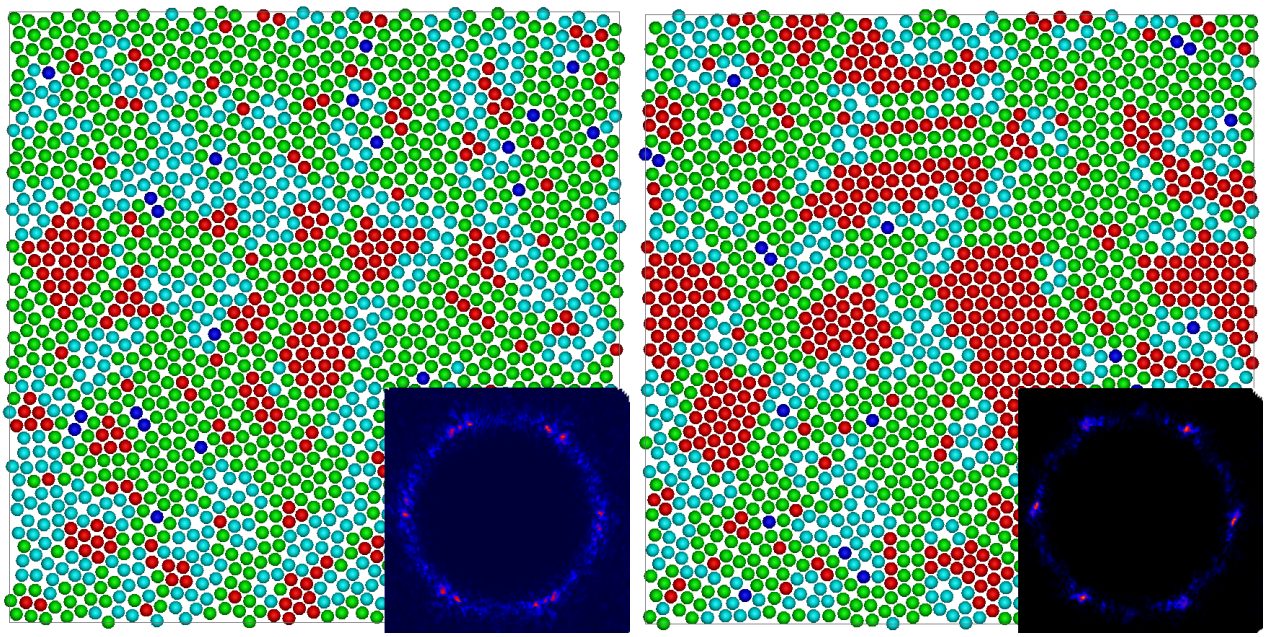

(a) $\beta p\sigma^3 = 30$

(b) $\beta p\sigma^3 = 40$

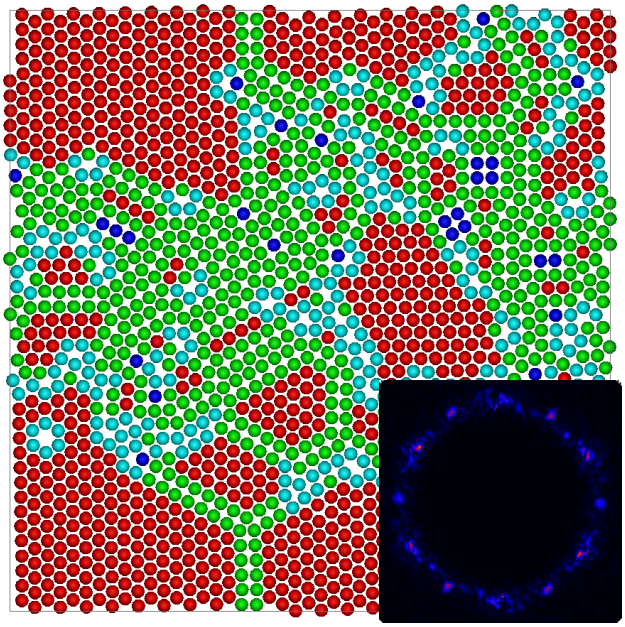

(c) $\beta p\sigma^3 = 60$

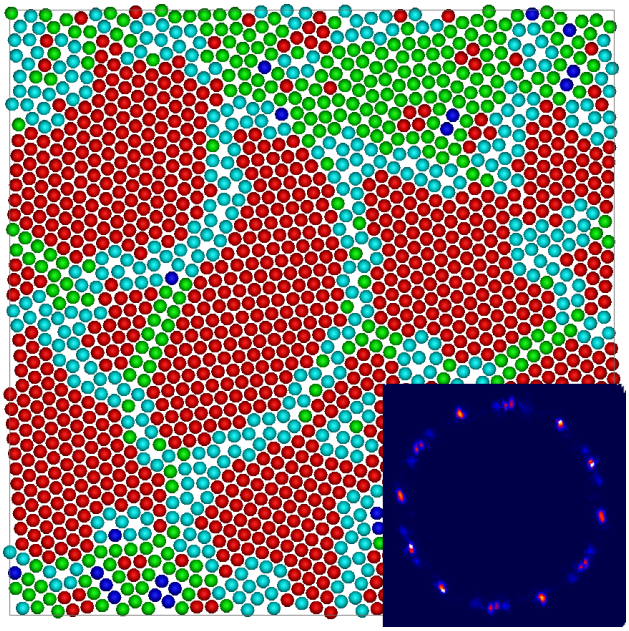

(d) $\beta p\sigma^3 = 90$

Figure 6.5: A selection of configurations for $\epsilon = 3$ at different pressures with the corresponding diffraction patterns for a system of $N = 1800$ particles.

are favored over Z particles. Unfortunately at these regions the density of the systems are too low to speak of a true crystal.The diffraction patterns also show a lack of discrete Bragg peaks in this region.

Because the results in Fig. 6.9. were obtained from many different simulations where we immediately started our simulation with increasingly higher pressures $p \in \{30 + 10n \mid 0 \leq n \leq 9\}$, we wanted to see if the defects were a result of this flash-compression, i.e. the method with which we simulated where we put a high pressure on the system instantly instead of gradually increasing the system. It is possible that the system will get stuck in an unfavorable configuration this way, especially since it was observed that the system dynamics were

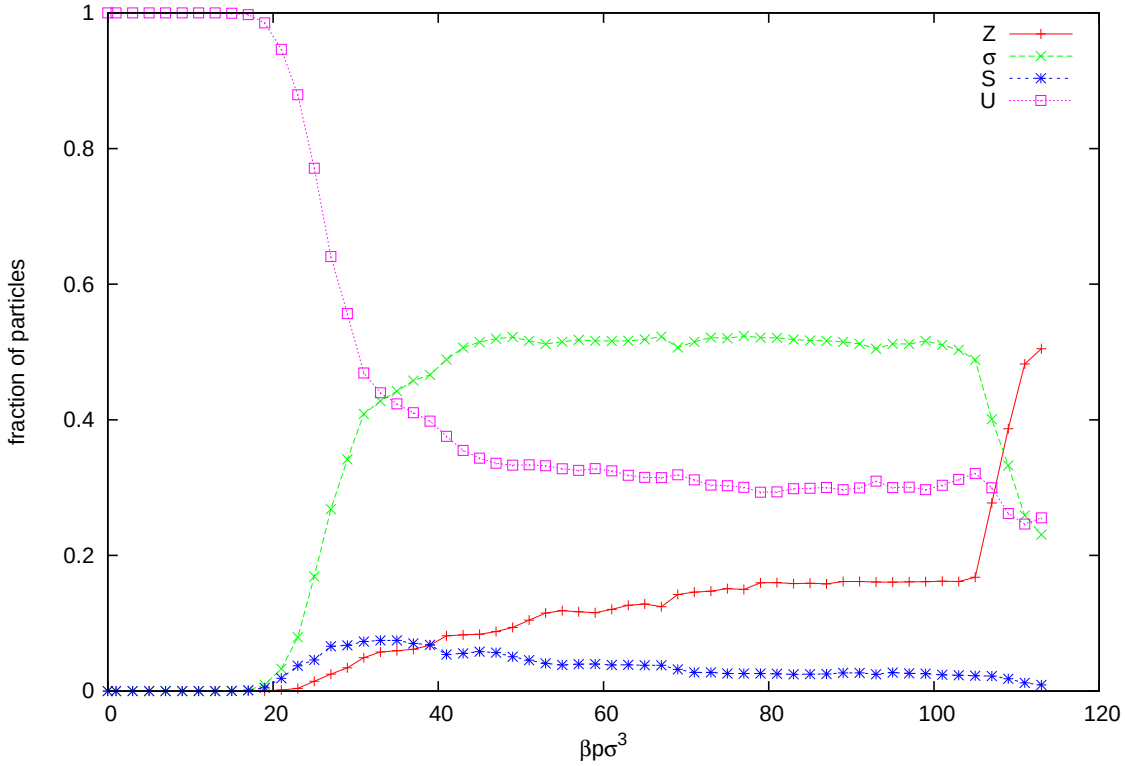

Figure 6.6: The fraction of particles of different types as a function of $\beta p\sigma^3$ for $\epsilon = 4$ for a system of $N = 1250$ particles with gradually increasing pressure.

rather slow. There were minimal changes over many tens of thousands of MCS. Because of computational limitations and the time in which this research had to be conducted we compared the results with those of a smaller system in which the pressure was gradually increased. The results for this system are shown in the particle-ratio plot in Fig. 6.8.

To make sure both systems were equibrilated we compared $E(t)$ plots where the 'time' is given by discrete MCS. For example the energy plot for $\epsilon = 5$ for $\beta p\sigma^3 = 100$ are shown below.

It is possible that the difference between the two systems of size $N = 1250$ and $N = 1800$ are because of finite size effects. From Fig. 6.10 we can tell that the system is at the very least almost equibrilated, however we cannot say for sure that there won't be jumps in the energy because the system dynamics are so slow. We have observed these jumps in other parts of the parameter space, for example for $\epsilon = 4$ where a hexagonal crystal formed rather abruptly (see also Fig. 6.6.) Longer simulation times, or a better algorithm are necessary to investigate this further.

6.5 Results for $\epsilon = 6$

While there is a large region where the ratio between σ and Z particles seem to allow for DDQC regions, the amount of unidentified particles here is far too high, which means that a large part of the system is still

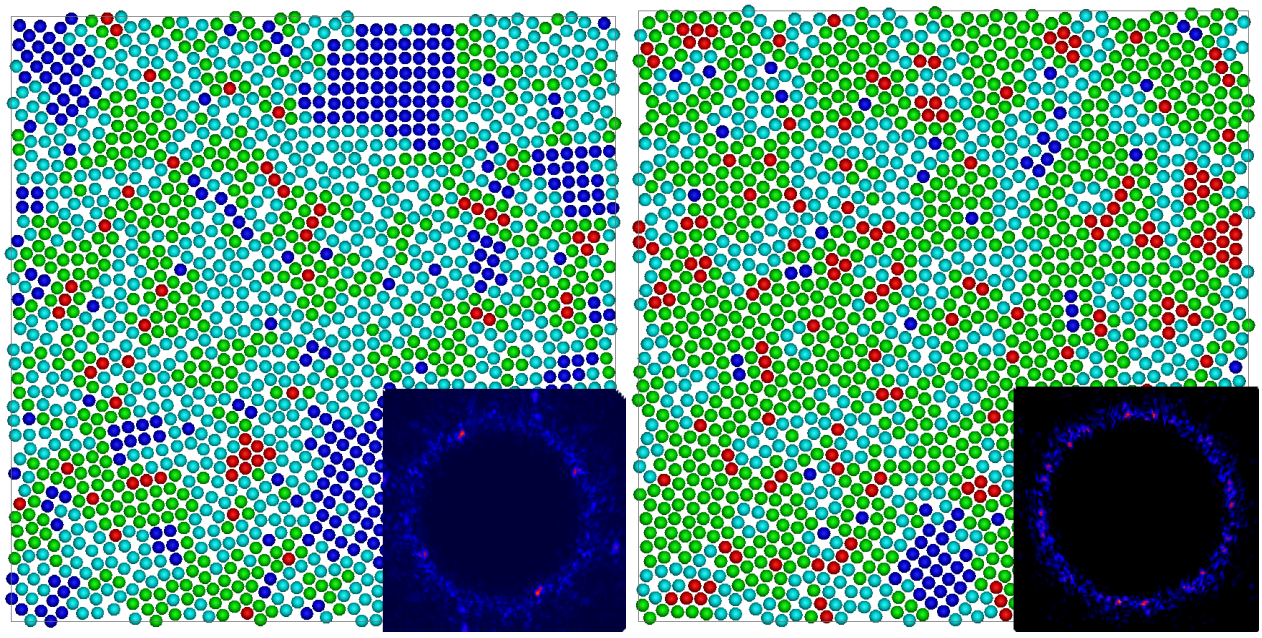

(a) $\beta p\sigma^3 = 28$

(b) $\beta p\sigma^3 = 38$

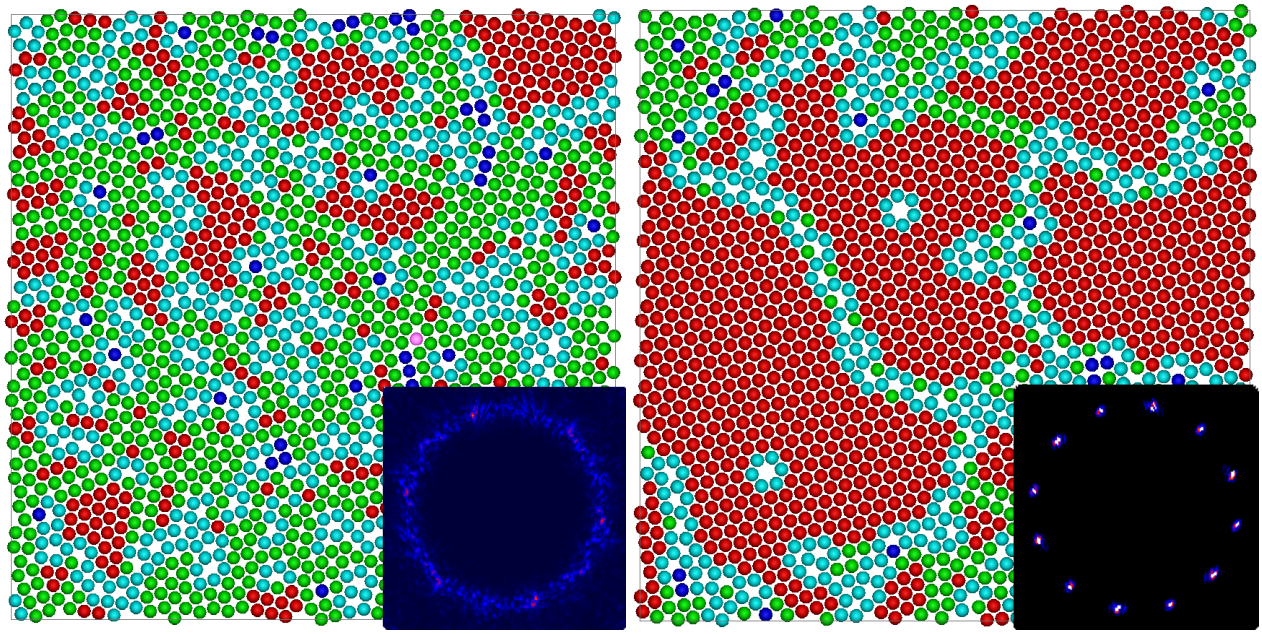

(c) $\beta p\sigma^3 = 65$

(d) $\beta p\sigma^3 = 180$

Figure 6.7: A selection of configurations for $\epsilon = 4$ at different pressures with the corresponding diffraction patterns for a system of $N = 1800$ particles.

fluid-like.

6.6 Results for $\epsilon = 8$

For higher energies $\epsilon \geq 8$ the system starts to behave increasingly like hard disks of diameter $\lambda\sigma$ in the region of interest, because the energy of the pair-interaction is high enough to counteract even the highest pressures.

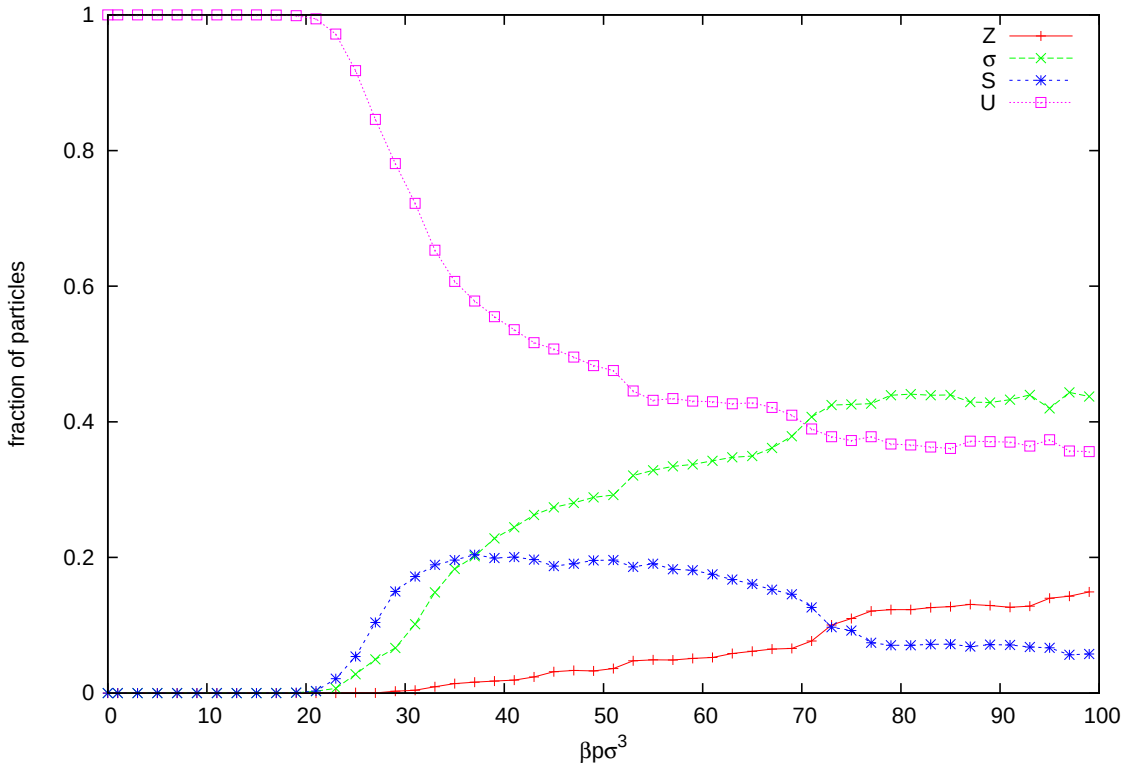

Figure 6.8: The fraction of particles of different types as a function of $\beta p\sigma^3$ for $\epsilon = 5$ for a system of $N = 1250$ particles with gradually increasing pressure.

6.7 Phase diagram

From the data obtained we constructed a tentative phase diagram. The results are shown in Fig. 6.14.

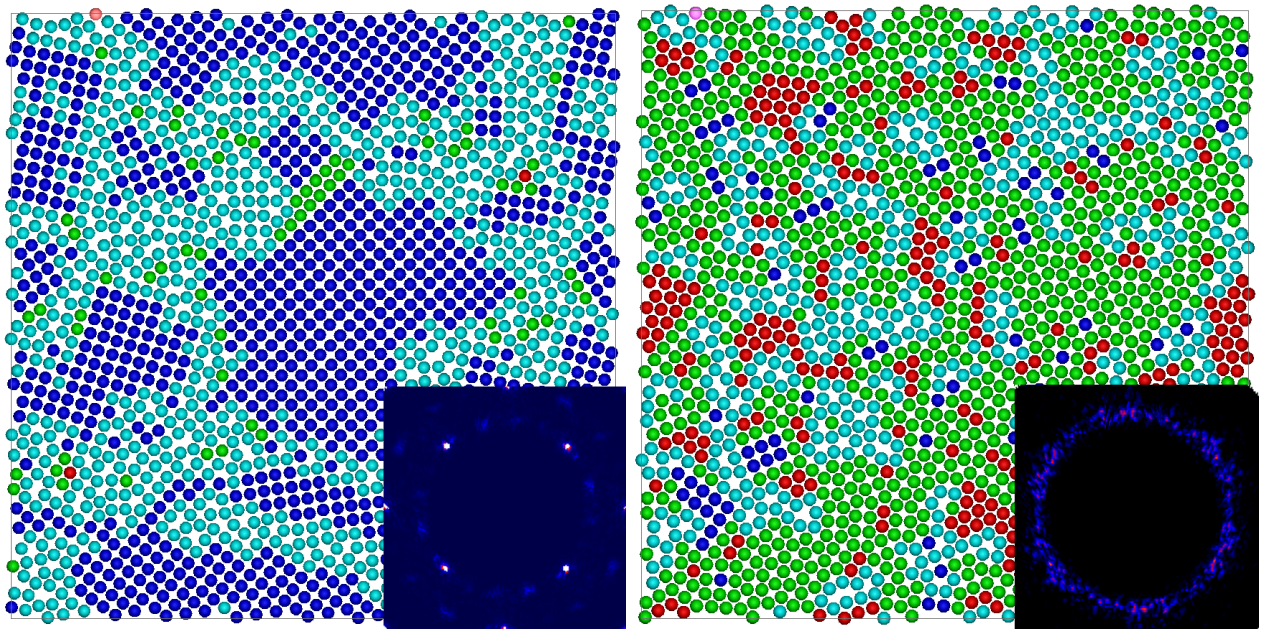

(a) $\beta p\sigma^3 = 30$

(b) $\beta p\sigma^3 = 70$

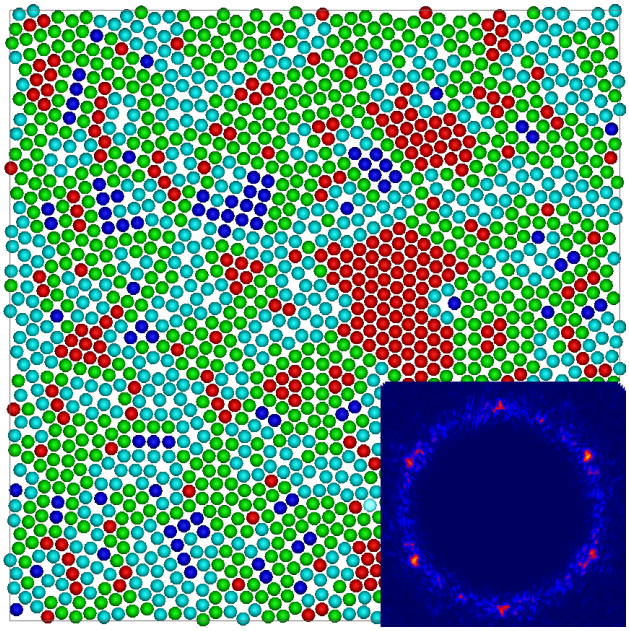

(c) $\beta p\sigma^3 = 100$

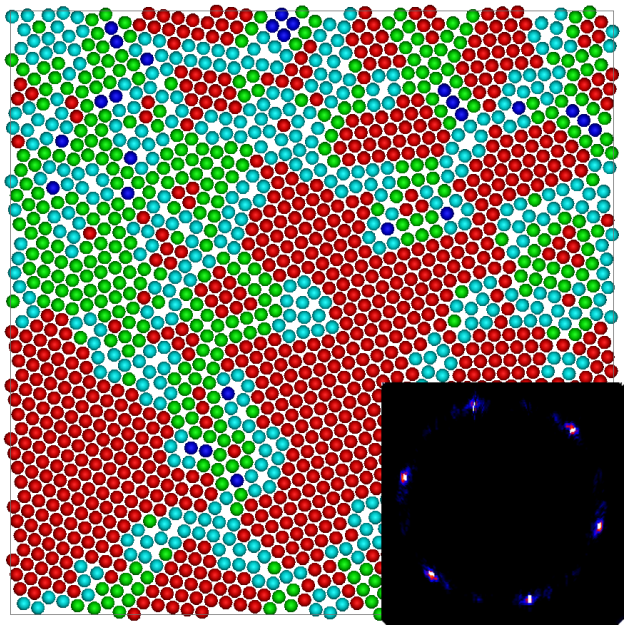

(d) $\beta p\sigma^3 = 150$

Figure 6.9: A selection of configurations for $\epsilon = 5$ at different pressures with the corresponding diffraction patterns for a system of $N = 1800$ particles.

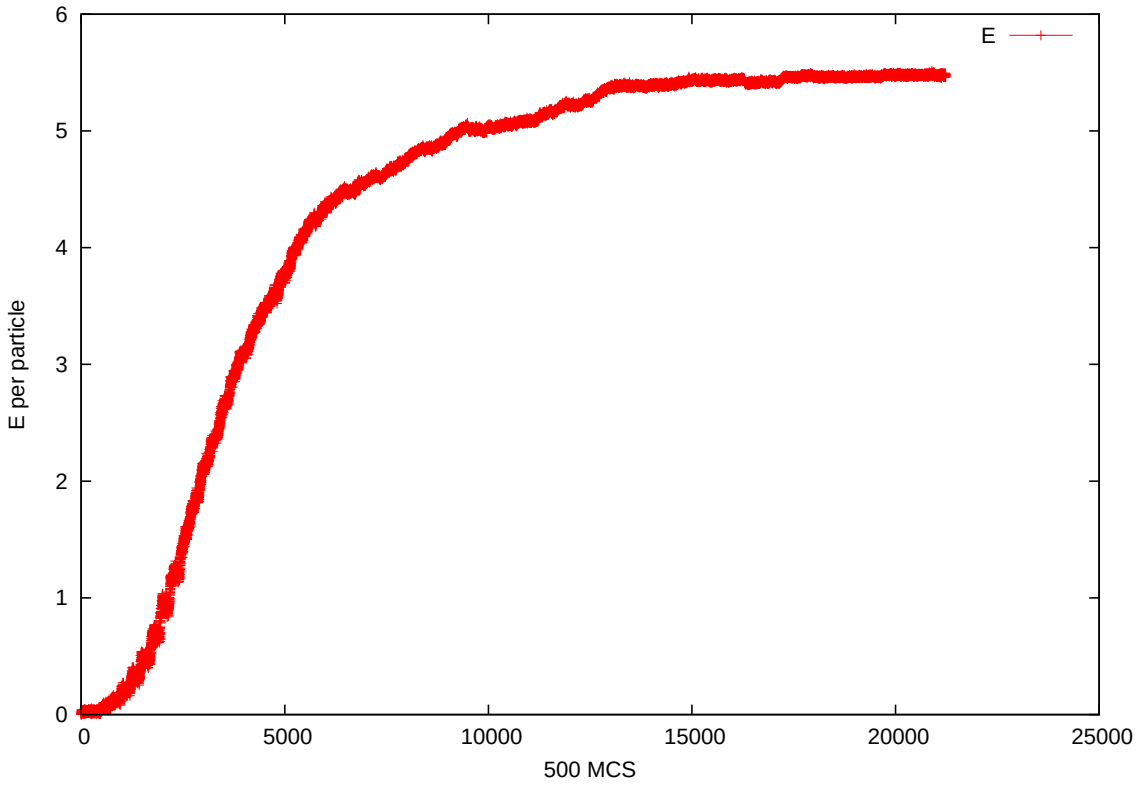

Figure 6.10: The energy per particle as a function of MCS for a single simulation run where $\epsilon = 5$ and $\beta p \sigma^3 = 100$.

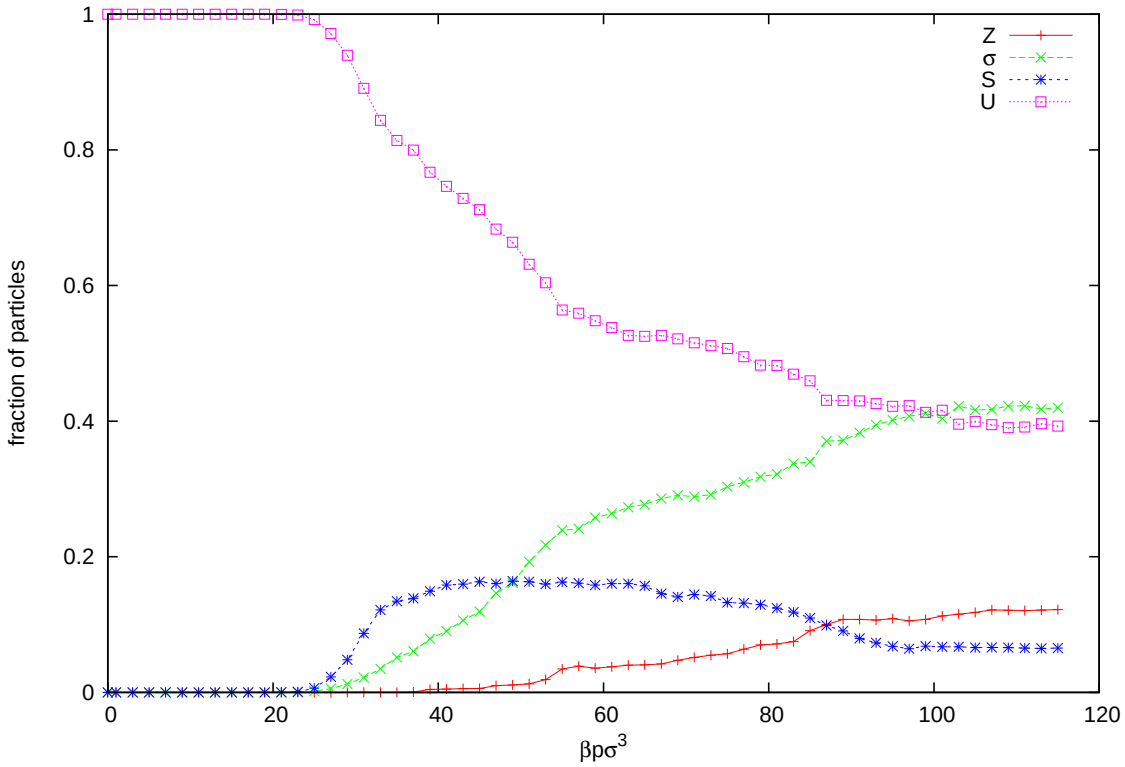

Figure 6.11: The fraction of particles of different types as a function of $\beta p\sigma^3$ for $\epsilon = 6$ for a system of $N = 1250$ particles with gradually increasing pressure.

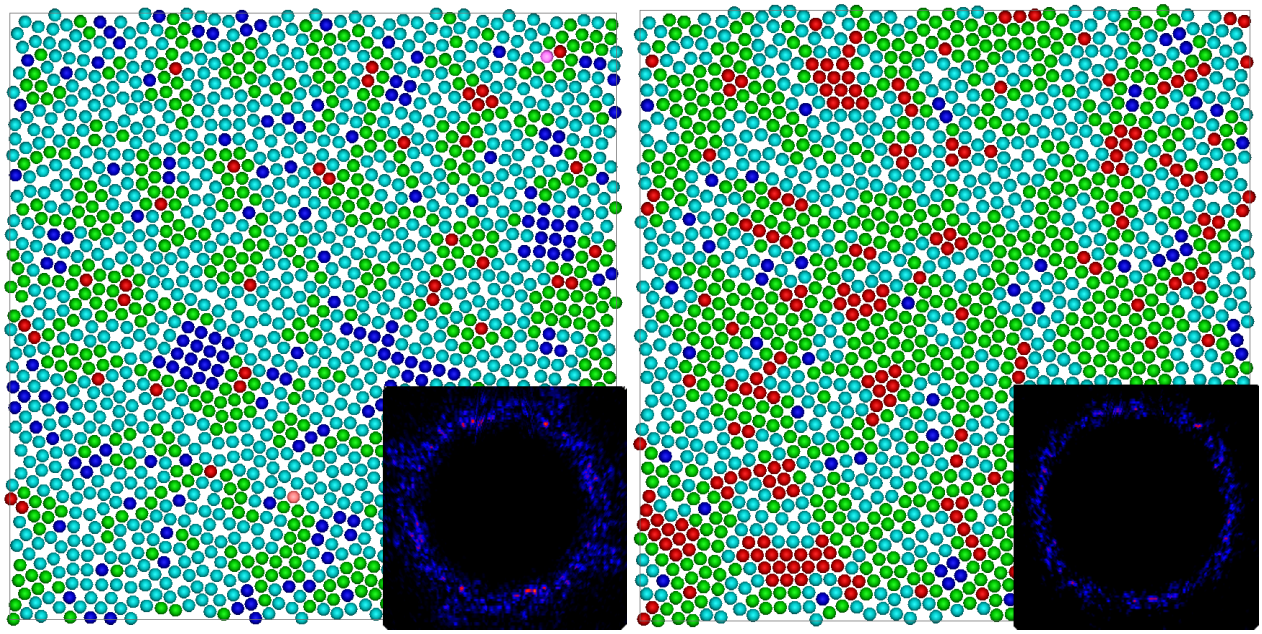

(a) $\beta p\sigma^3 = 48$

(b) $\beta p\sigma^3 = 82$

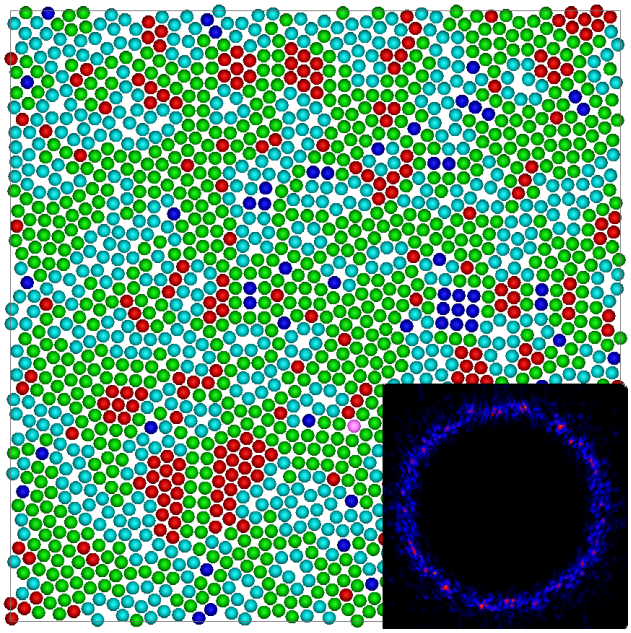

(c) $\beta p\sigma^3 = 98$

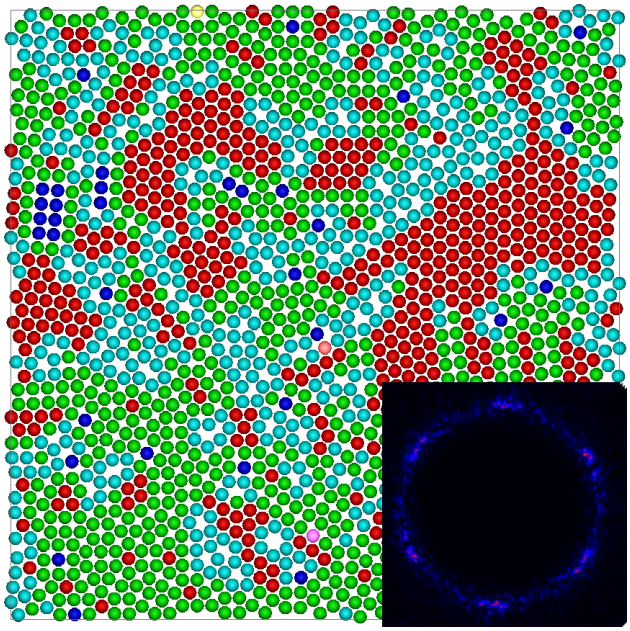

(d) $\beta p\sigma^3 = 148$

Figure 6.12: A selection of configurations for $\epsilon = 6$ at different pressures with the corresponding diffraction patterns for a system of $N = 1800$ particles.

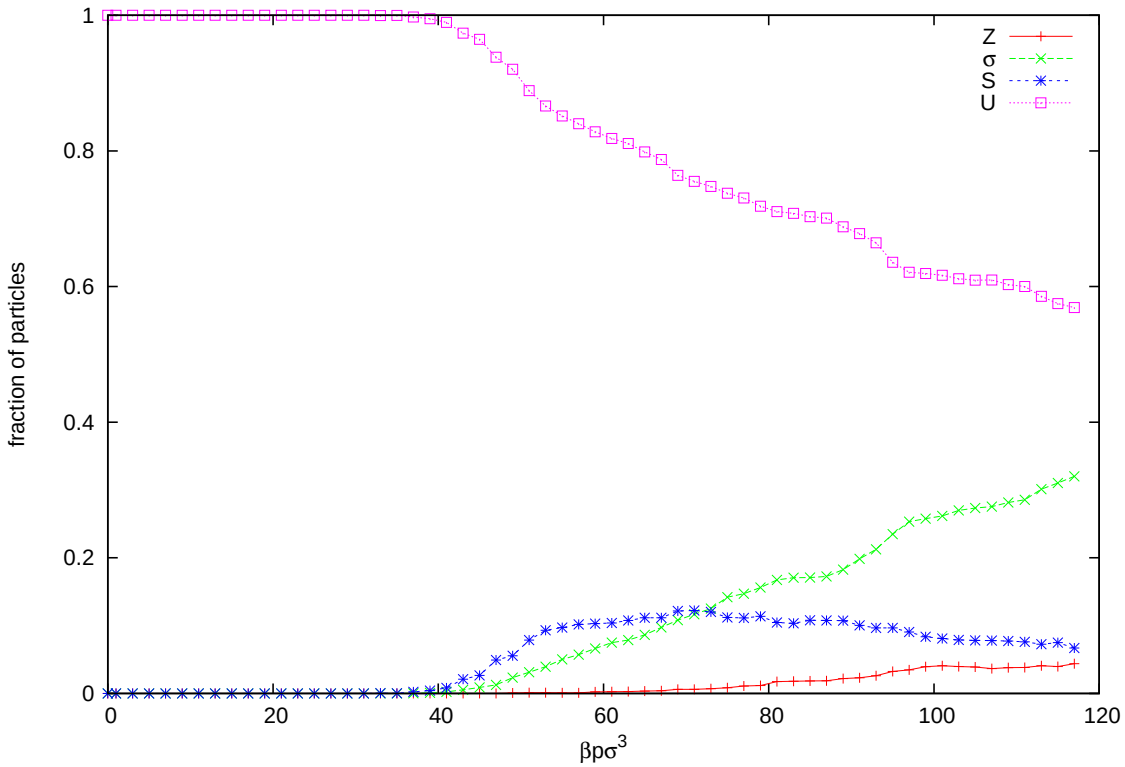

Figure 6.13: The fraction of particles of different types as a function of $\beta p\sigma^3$ for $\epsilon = 8$ for a system of $N = 1250$ particles with gradually increasing pressure.

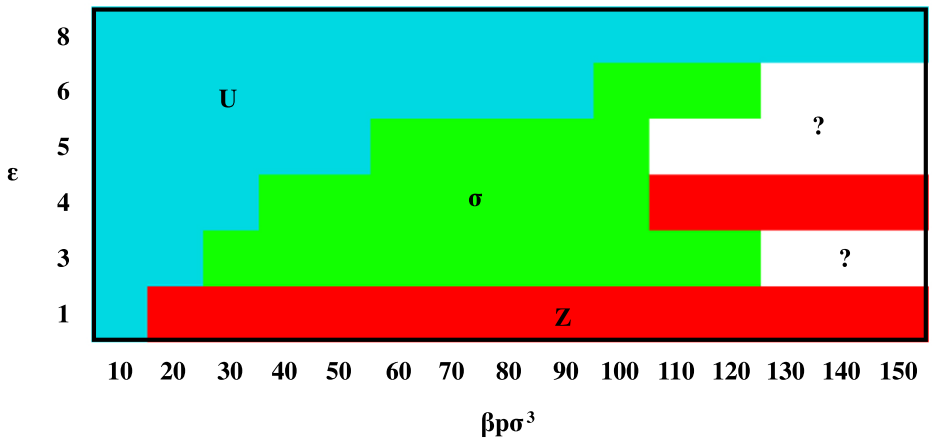

Figure 6.14: A phase diagram showing the predominant neighborhood for different regions of our parameter space. Compare with the particle ratio plots presented in this chapter.

Chapter 7

Discussion

7.1 Conclusion

The configurations and graphs presented in the previous chapter show that the system has a rich phase diagram. The energy ϵ of the two-body interaction seems to have a profound influence on the structure of the system. As we have seen, for low energy the system behaves like a system of hard disks, as expected. For higher energies we see that σ particles are increasingly favored over the other particles, in particular over the Z particles which are the predominant neighborhood in hard-disk systems, since they form the natural crystal in this system.

While we did not find any quasicrystalline regions, some configurations clearly showed dodecagonal elements. Furthermore we did find polycrystalline configurations that showed 12-fold diffraction patterns. We would expect a DDQC to form in a region where the ratio of σ particles to Z particles is well in favor of the σ particles. We see that the regions of the parameter space that show clear dodecagonal patterns coincide with the regions where the particle-ratio graphs show a $\sigma - Z$ ratio of about 4. It is therefore our expectation that a DDQC may very well be stable under this pair-potential. However as we mentioned the system dynamics were slow and we were unable to equibrilate the system in the time in which this research was conducted. There is an indication that DDQC would be stable in the aforementioned regions, and we expect that with larger simulation times these configurations might self-assemble.

The way in which we analyzed the parameter space, by looking at particle ratios, seems to be a very good indicator of quasicrystalline regions, especially when combined with diffraction patterns.

7.2 Outlook

Self-assembly seems to be a significant obstacle in simulations of quasicrystals using a repulsive pair-potential. There is a clear indication that a DDQC phase may exist for a system of hard-disks with a square-shoulder potential. Future research will need a better algorithm or longer simulation times to explore this possibility further. It would also be very useful to explore the stability of an ideal DDQC under this pair-potential. Looking further, it would also be interesting to see if it is possible to replicate the experimental results of [6] with a similar setup but with a binary mixture of particles. It would be especially interesting to see if we get the same results for the particle-size ratio γ that favors DDQC regions, which was mentioned in [6] to be around $\gamma \approx 0.42$ for a variety of systems.

Bibliography

[1] Shephard, B. G. A. G. C. (1977). Tilings and Patterns (Presumed First.). W. H. Freeman and Company.

[2] van der Linden, M. N., Doye, J. P. K., & Louis, A. A. (2012). Formation of dodecagonal quasicrystals in two-dimensional systems of patchy particles. The Journal of Chemical Physics, 136(5), 054904. doi:10.1063/1.3679653

[3] Janot, C. (2012). Quasicrystals: A Primer (Oxford Classic Texts in the Physical Sciences) (2nd ed.). Oxford University Press, USA.

[4] Oxborrow, M., & Henley, C. L. (1993). Random square-triangle tilings: A model for twelvefold-symmetric quasicrystals. Physical Review B, 48(10), 6966.

[5] Haji-Akbari, A., Engel, M., Keys, A. S., Zheng, X., Petschek, R. G., Palffy-Muhoray, P., & Glotzer, S. C. (2009). Disordered, quasicrystalline and crystalline phases of densely packed tetrahedra. Nature, 462(7274)

[6] Talapin, D. V., Shevchenko, E. V., Bodnarchuk, M. I., Ye, X., Chen, J., & Murray, C. B. (2009). Quasicrystalline order in self-assembled binary nanoparticle superlattices. Nature, 461(7266)

[7] Armstrong M.A. (1987). Groups and Symmetry. Undergraduate Texts in Mathematics. Springer.

[8] Blundell S. & K. Concepts in Thermal Physics. Oxford University Press.

[9] Berend Smit, D. F. (2010). Understanding Molecular Simulation, Second Edition (Computational Science Series, Vol 1)

[10] Dijkstra M. Lecture Notes, Computational Soft Condensed Matter.

[11] M. Senechal, "Crystalline symmetries: An informal mathematical introduction" (Adam Hilger, Bristol, 1990).